Geological Field Trips and Maps

A field guide to the excursion in the Maures Massif (southern France): a complete transect of the Southern European Variscan belt

2022
Vol. 14 (2.1)

ISSN: 2038-4947

https://doi.org/10.3301/GFT.2022.04

GFT&M - Geological Field Trips and Maps

Periodico semestrale del Servizio Geologico d'Italia - ISPRA e della Società Geologica Italiana
Geol. F. Trips Maps, Vol.**14** No.2.1 (2022), 41 pp., 25 Figs., 1 tab. (https://doi.org/10.3301/GFT.2022.04)

A field guide to the excursion in the Maures Massif (southern France): a complete transect of the Southern European Variscan belt

Matteo Simonetti[1]

[1] Servizio Geologico d'Italia, ISPRA, 00144 Roma, Italy.

Corresponding Author e-mail address: matteo.simonetti@isprambiente.it

Cover page Figure: View of the chloritoid-bearing micaschist at the Plage du Cobasson (Photo courtesy of Matteo Simonetti).

ISSN: 2038-4947 [online]

http://gftm.socgeol.it/

https://doi.org/10.3301/GFT.2022.04

Index

Information

Excursion notes

Itinerary

https://doi.org/10.3301/GFT.2022.04

Abstract

In this guide key outcrops of the Maures Massif, the southernmost part of the Variscan belt in France, are described. Here the features acquired during the fundamental steps of the evolution of the southern European Variscan belt can be recognised. The field trip develops along a W to E transect, perpendicular to the main architecture of the belt. It is organised in eight stops that can be easily reached by car or by walking. The excursion can be completed in one day, but to better enjoy these spectacular outcrops, two days are suggested. The stops show significative outcrops of the low-grade rocks of the External Zone up to the high-grade migmatite of the Internal Zone. Particular focus is given on the tectonic contact between the Internal and External zones of the belt marked by a km-scale transpressional shear zone, known as the Cavalaire Fault, whose structural, lithological, metamorphic and geochronological aspects are described in detail. This structure is a branch of a crustal-scale system of late Carboniferous shear zones known at the regional-scale as the East Variscan Shear Zone. The several branches were interconnected and all recorded a common evolution characterised by transpressional deformation starting from ~330 My.

Keywords
Maures–Tanneron Massif, East Variscan Shear Zone, Monazite petrochronology, Cavalaire Fault, Transpression.

Program Summary

The field trip develops along eight stops that can be visited in one day. However, it is suggested to divide the excursion in two parts in order to complete the excursion in two days. Most of the outcrops are located along the coast and there is no particular danger or difficulty to reach them. It should be noted that during summer the stop locations are generally very crowded because of tourists and, in this period, many of the available parking slots are subject to charges. The stops are organised in order to show a W to E transect of the Variscan belt of the Maures Massif starting from the low-grade rocks of the External Zone up to the high-grade migmatite of the Internal Zone with a detailed focus on the tectonic contact between them that is marked by a ductile mylonitic shear zone.

https://doi.org/10.3301/GFT.2022.04

Stop	Location	Latitude	Longitude	height (m)
1	External Zone, chloritoid-bearing micaschist at Cobasson village	43°06’02.8”N	006°19’20.6”E	0
2	External Zone, Bormes orthogneiss and kyanite-bearing micaschist	43°08’21.0”N	006°22’52.6”E	0
3	Transition Zone, staurolite-bearing micaschist of the Cavalaire Fault at Col du Canadel	43°10’09.1”N	006°28’29.0”E	270
4	Transition Zone, mylonitic gneiss of the Cavalaire Fault	43°11’11.0”N	006°30’08.5”E	425
5	Transition Zone, mylonitic migmatite of the Cavalaire Fault at Cavalaire sur-Mer	43°10’07.8’’N	006°32’23.4’’E	0
6	Internal Zone, mylonitic garnet-bearing micaschist	43°11’11.2”N	006°35’11.5”E	0
7	Internal Zone, unsheared migmatite	43°12’41.5’’N	006°38’09.5’’E	20
8	Internal Zone, relations between the migmatites and the Plan de la Tour granite	43°18’ 01.6’’N	006°33’26.4’’E	150

Table 1 - Summary of number, location, latitude, longitude and altitude of the stops of the field trip.

Safety

Outcrops can be easily reached by car or by easy walking with no particular access difficulties. Some of the stops are located along coastal rocks, therefore adequate shoes are required. The field trip can be completed during all periods of the year thanks to the weather that is generally good and rarely too cold.

Hospitals

Hospital De Saint-Tropez, Rd559, 83580 Gassin, France - Ph. +33 4 98 12 50 00

Accommodation

There are several hotels, B&B, and camping in the area of the field. According to the field trip schedule, it is suggested to book an accommodation in Cavalaire-sur-Mer or in La Croix-Valmer villages in order to divide the field trip in two days.

https://doi.org/10.3301/GFT.2022.04

1. Introduction

Complete sections of orogens are not so commonly exposed especially when dealing with ancient orogenic belts that are usually eroded and/or overprinted by subsequent tectonic activity. Detailed studies of the tectonic and metamorphic histories of orogens along structural profiles provide fundamental data disclosing their usually complex and polyphase evolution. The Maures Massif in southern France, in the area between Saint Tropez and Bormes, is the location of this field trip. Similarly to northern Sardinia, this massif provides the opportunity to directly observe a complete section of the Southern European Variscan belt that mostly escaped the subsequent alpine tectonics. Here, along a 25 km W to E transect it is possible to observe the transition from low-grade rocks of the external part of the belt (External Zone) to the high-grade migmatitic rocks of the metamorphic core (Internal Zone). Furthermore an important transpressional high strain zone marking the contact between the two zones crops out.
In this guide some of the key outcrops of the Maures Massif are described. In these selected localities fundamental steps of the evolution of the southern European Variscan belt can be recognised. This transect was widely studied from several points of view. The tectono-metamorphic evolution of this section of the belt is well constrained (Bellot, 2005; Corsini and Rolland, 2009; Schneider et al., 2014; Oliot et al., 2015; Gerbault et al., 2018). Recently, new structural and geochronological data collected from the Transition Zone between the External and Internal zones provided new insights on the late Variscan evolution of this sector of the belt. These new observations help also to improve possible palaeogeographic correlations with the other fragments of Variscan belt in the Mediterranean area (Simonetti et al., 2020a).

2. Geology of the Variscan belt

The Variscan belt is the result of the continent-continent collision between Laurentia-Baltica and Gondwana (Fig. 1a) that occurred between 380 My and 280 My (Arthaud and Matte, 1977; Burg and Matte, 1978; Tollmann, 1982; Matte, 1986, 2001; Di Vincenzo et al., 2004). This collision probably involved two microplates (Avalonia and Armorica) and led to the assemblage of Pangea with the formation of a mountain system extending from North America up to Caucasus (Matte, 2001). Palaeomagnetic and palaeobiostratigraphic methods allowed to distinguish the Iapetus Ocean between Avalonia and Laurentia and the Rheic Ocean between Avalonia and the Armorica microplate (Matte, 2001 and references therein).

https://doi.org/10.3301/GFT.2022.04

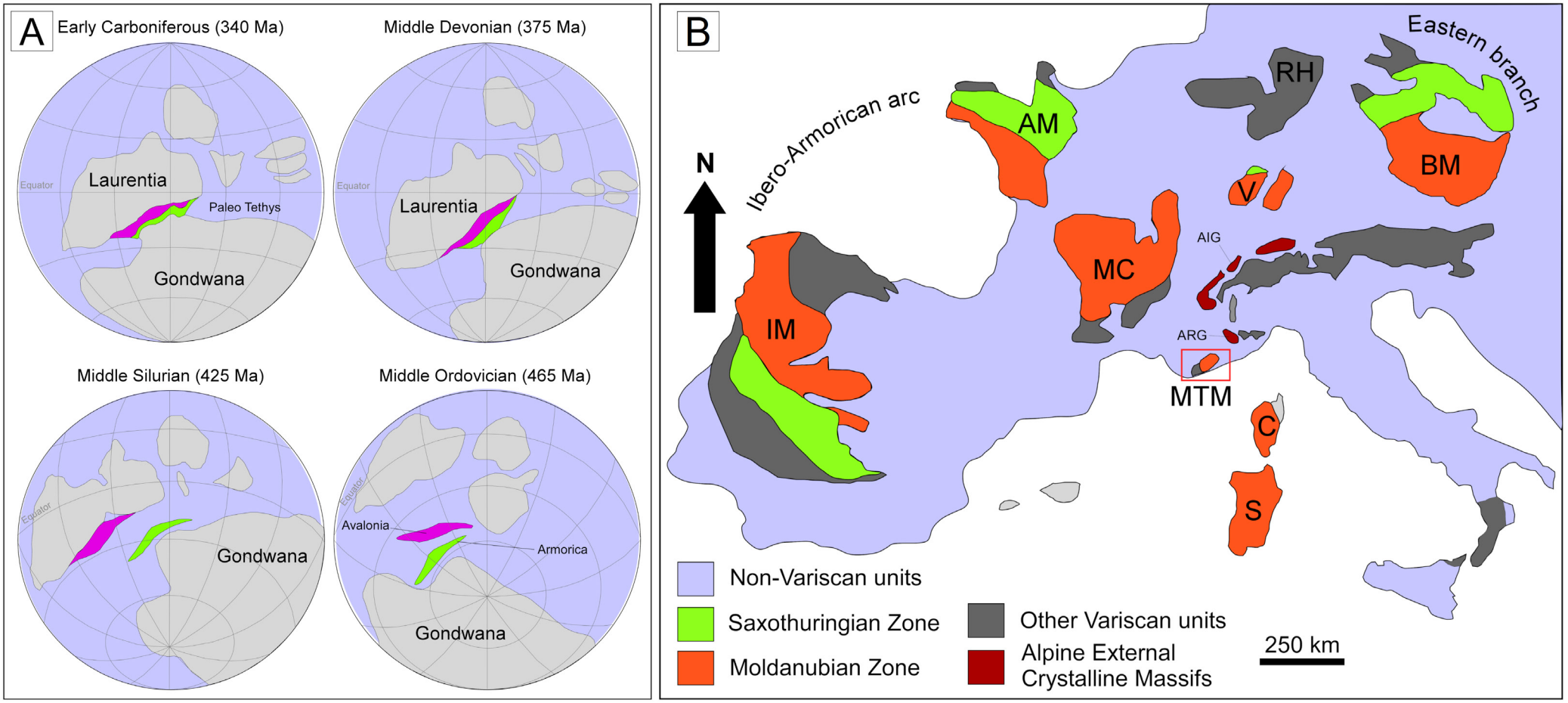

Fig. 1 - A) Palaeozoic reconstruction from Middle Ordovician to early Carboniferous (modified after Matte, 2001) showing the collision between Laurentia and Gondwana; B) Present-day distribution of the Variscan units in Europe (modified after Compagnoni et al., 2010); AM = Armorican Massif; BM = Bohemian Massif; C = Corsica; IM = Iberian Massif; MC = Massif Central; MTM = Maures-Tanneron Massif; RH = Rheno-Hercynian; S = Sardinia; V = Vosges; red box indicates the study area.

The Variscan belt in Europe is also known as the Variscides. In this sector of the belt (Fig. 1b; Fluck et al., 1991; Matte, 2001; Ballèvre et al., 2009; Faure et al., 2009; Skrzypek et al., 2012), the Saxothuringian Zone (southwestern Iberian Massif, northern Armorican Massif, Vosges and Bohemian Massifs) and the Moldanubian Zone (southern Iberian Massif, central and southern Vosges, Central Massif, southern Armorican Massif, and southern Bohemian Massif) are recognised according to the structural and metamorphic evolution during the

https://doi.org/10.3301/GFT.2022.04

collision and taking into account the recognised oceanic sutures. The Moldanubian Zone is considered as the metamorphic root of the belt (Schulmann et al., 2009).

The Variscides are a composite orocline showing two large scale arcs (Fig. 1b; Matte, 2001) involving all the main domains of the belt. A western branch, the Iberian-Armorican arc (Arthaud and Matte, 1977; Dias and Ribeiro, 1995; Dias et al., 2016; Fernández-Lozano et al., 2016), and a nameless smaller eastern branch (Matte, 2001; Bellot, 2005; Ballèvre et al., 2018; Simonetti et al., 2020b) are recognised. Some Authors proposed that the eastern arc was delimited by a regional-scale system of dextral transpressive shear zones known as the East Variscan Shear Zone (Fig. 2; EVSZ; Corsini and Rolland, 2009; Carosi et al., 2012, 2020; Padovano et al., 2012, 2014; Simonetti et al., 2018, 2020b).

Because of the subsequent Alpine orogenesis, the south-eastern sector of the Variscan belt was fragmented and partially overprinted by Alpine tectonics and metamorphism (Stampfli and Kozur, 2006). This lead to unclear interpretation of the spatial extension, timing and role of the EVSZ and to contrasting palaeogeographic reconstructions of this area of the belt (Stampfli et al., 2002; Advokaat et al., 2014). In particular, the lateral relationships between the Corsica-Sardinia Block, the Maures-Tanneron Massif, and the Variscan basement of the Western Alps (External Crystalline Massifs) still debated. The correlation between those sectors is mostly based on lithological and stratigraphic affinities and palaeomagnetic data. In particular, it is not clear if the

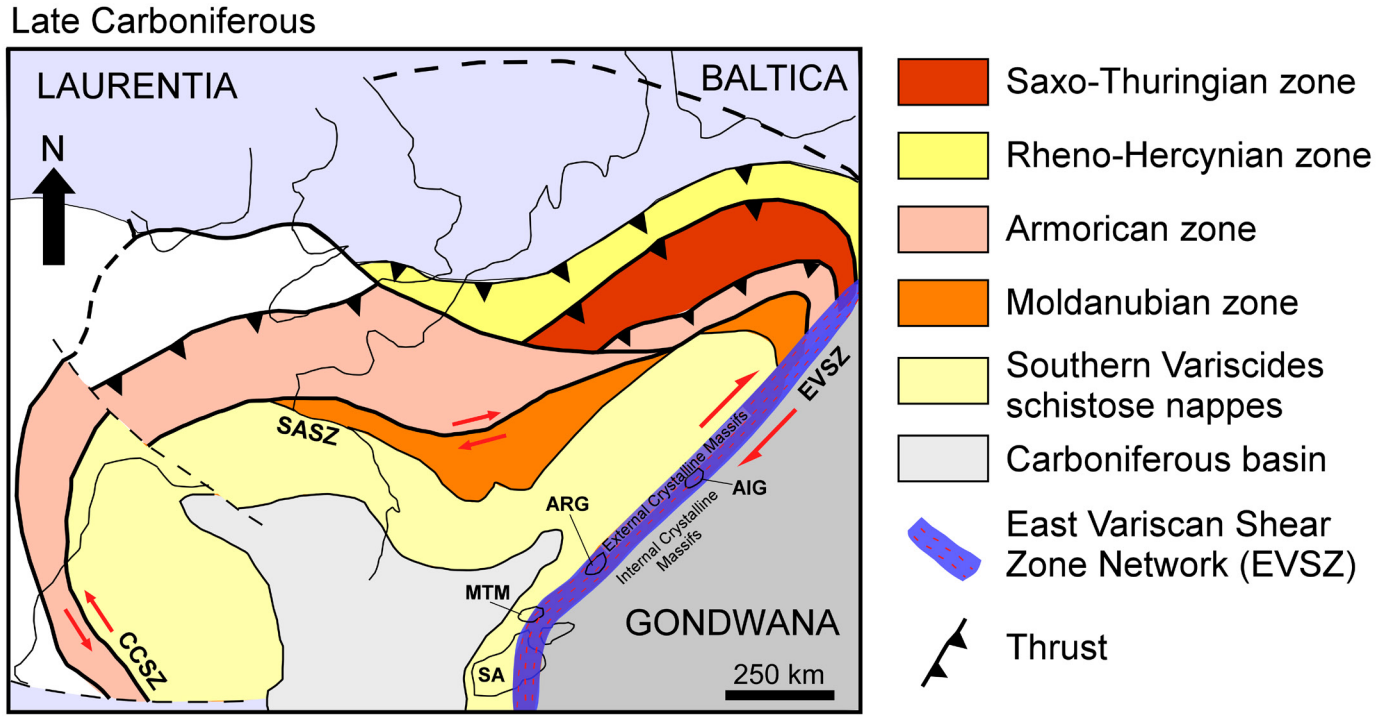

Fig. 2 - Reconstruction of the Variscan belt during late Carboniferous (modified after Guillot and Ménot, 2009; Carosi et al., 2012). AIG: Aiguilles Rouge Massif; ARG: Argentera Massif; CCSZ: Coimbra-Cordoba Shear Zone; MTM: Maures-Tanneron Massif; SA: Sardinia; SASZ: South Armorican Shear Zone.

https://doi.org/10.3301/GFT.2022.04

Corsica-Sardinia Block was connected to Iberia (Stampfli et al., 2002; Turco et al., 2012) or to southern France (Rosenbaum et al., 2002; Advokaat et al., 2014) during the late Carboniferous times. Recently, Simonetti et al. (2018, 2020a, 2020b) and Carosi et al. (2020) provided new structural and geochronological data from the Alpine External Crystalline Massifs, from northern Sardinia, and from the Maures Massif that better define the extension of the EVSZ and that directly constrained the timing of its activity during late Carboniferous time (~320 My, U-Th- Pb on monazite).

3. Geological setting of the Maures-Tanneron Massif

The Maures-Tanneron Massif (MTM) is the southernmost segment of the Variscan belt in France (Fig. 1b; Matte, 2001; Compagnoni et al., 2010). The MTM is composed of low- to high-grade metamorphic rocks, the latter intruded by Carboniferous granitoids (Fig. 3; Crevola and Pupin, 1994). The Maures Massif is separated from the Tanneron Massif by the E-W trending Permian Esterel basin (Fig. 3).

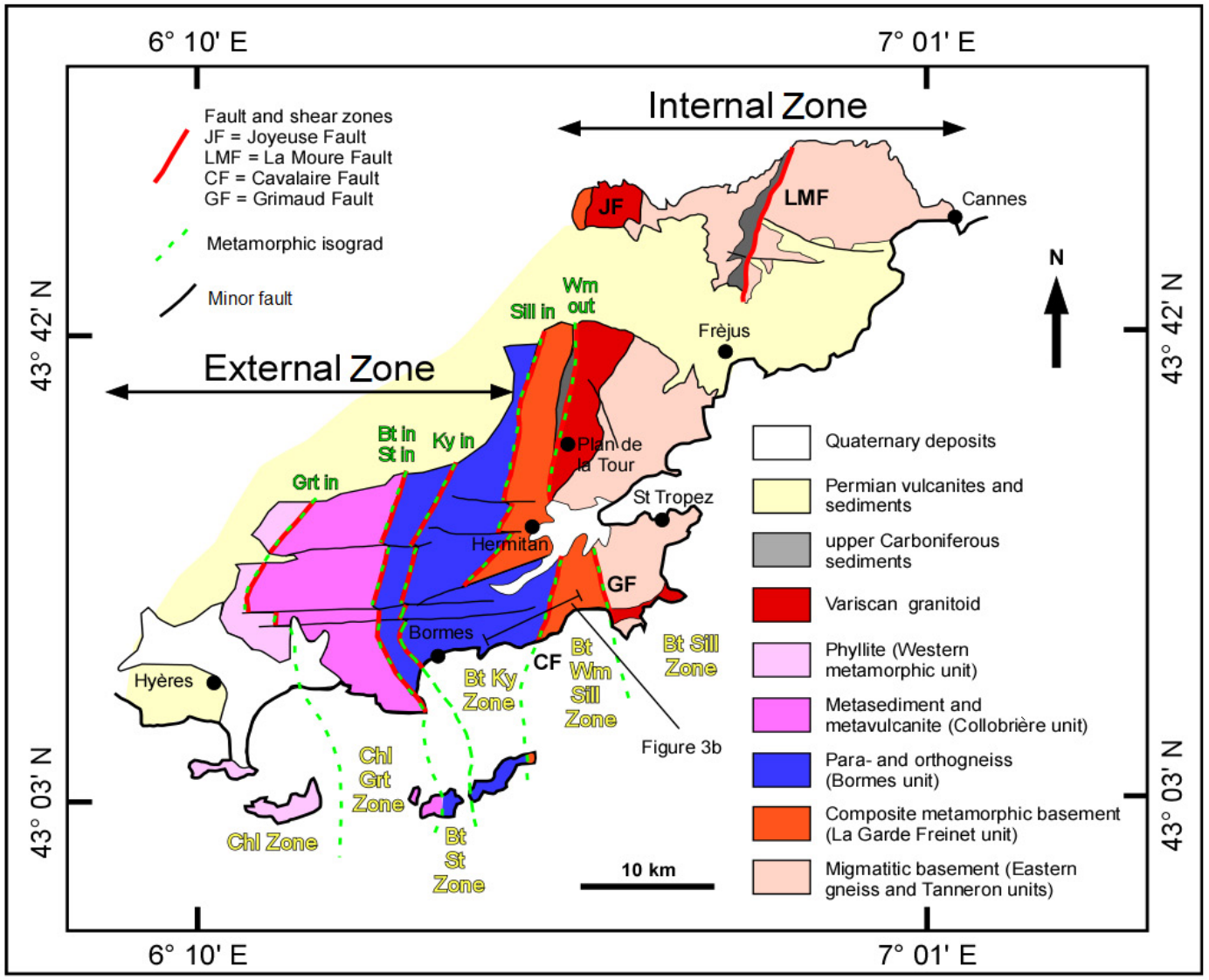

Fig. 3 - Geological sketch map of the Maures-Tanneron Massif (modified after Bellot, 2005; Compagnoni et al., 2010; Schneider et al., 2014; Oliot et al., 2015; Gerbault et al., 2018; Simonetti et al., 2020a).

https://doi.org/10.3301/GFT.2022.04

The western domain of the MTM records a 360-330 My old collisional Barrovian metamorphism increasing in grade from west to east (Bellot, 2005; Corsini and Rolland, 2009; Compagnoni et al., 2010; Schneider et al., 2014; Oliot et al., 2015). Several Variscan metamorphic units are distinguished (see review in Schneider et al., 2014; Fig. 3a). From W to E, the main units are: 1) the Western metamorphic unit (Fig. 3) consist of lower Palaeozoic low-grade phyllite belonging to the chlorite zone; 2) the Collobrières unit (Fig. 3), deformed within the garnet-chlorite zone, consisting of iron-rich metasediments (quartzite, marble and gneiss) and metavolcanic rocks (also known in the literature as leptyno-amphibolitic complex) interpreted as a volcano-sedimentary suite emplaced during Cambrian continental rifting (Briand et al., 2002; Innocent et al., 2003); 3) the Bormes unit (Fig. 3), made of the Bormes orthogneiss and associated metasediments, affected by Barrovian metamorphism from the biotite-staurolite zone up to the biotite-kyanite zone; 4) the La Garde-Freinet unit (Fig. 3) containing micaschist, migmatitic paragneiss and orthogneiss with acid, mafic, and ultramafic lenses (represented by an association of amphibolite and metavolcanic rocks). This unit corresponds to the sillimanite-biotite zone of the Barrovian metamorphic sequence; 5) the Eastern Gneiss and Tanneron units (Fig. 3), affected by metamorphism in the sillimanite-biotite zone, are made of migmatitic ortho- and paragneiss with associated mafic eclogite lenses showing a polyphase metamorphism. Eclogitic bodies represent the remnants of a dismembered suture zone now embedded within the migmatites (Schneider et al., 2014). A minimum age of 430 My for eclogitisation of metabasites was obtained by Moussavou (1998) using U–Pb dating on zircon. The La Garde-Freinet and Eastern Gneiss units are intruded by syn-kinematic calc-alkaline and peraluminous granitoids (Fig. 3): the Hermitan granite (in the La Garde-Freinet unit) and the Plan de la Tour granite (in the Eastern Gneiss unit), the last one cropping out in the core of a regional-scale N-S trending antiform (Rolland et al., 2009). The Western metamorphic unit together with the Collobrière unit and the Bormes unit are included in the External Zone. The La Garde-Freinet, Eastern Gneiss and Tanneron units are part of the Internal Zone (Fig. 3) characterised by several episodes of widespread post-collisional partial melting (~650-700 °C and 5-8 kbar; Buscail, 2000) and syn-tectonic granitic intrusions within the cores of regional scale antiforms (Schneider et al., 2014).

The units of the External Zone record the collisional stage and nappe staking while the units of the Internal Zone record the post-collisional transpressional tectonics coupled with anatexis and exhumation of the lower crust.

In the past years a debate regarding the main structure that separates the External and Internal zones occurred. It is now clear that the Cavalaire Fault (CF; Figs. 3 and 4), affecting both micaschist of the biotite-kyanite zone and migmatites, is a transition zone between the External and Internal Zones (Schneider et al., 2014;

https://doi.org/10.3301/GFT.2022.04

Simonetti et al., 2020a). Schneider et al. (2014) recognised several tectono-metamorphic stages in the Maures Massif. In particular there is evidence of a Siluro-Devonian subduction followed by a collisional stage that is well preserved in the External Zone. Subsequently, the exhumation of the tectonic units occurred in the context of a transpressive regime, similar to the D_2 phase recognised in northern Sardinia, coupled with extensive anatexis in the Internal Zone (Schneider et al., 2014).

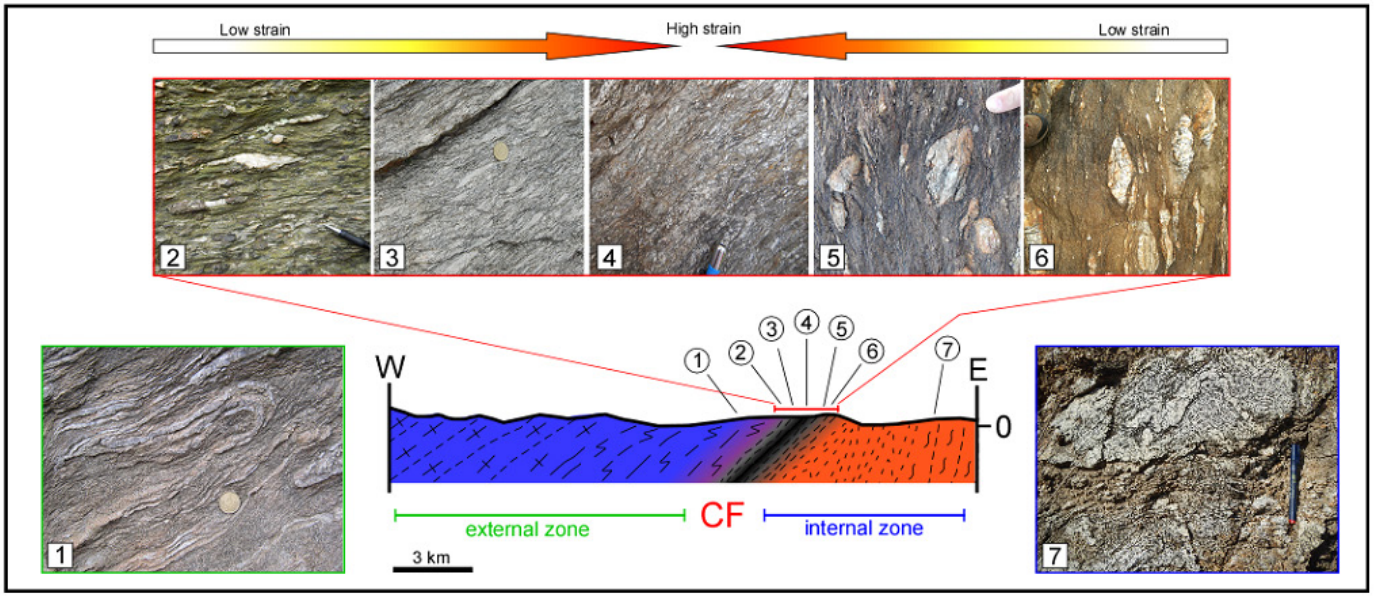

Fig. 4 - Schematic cross-section across the contact between the Internal and External zones (location is reported in Fig. 3) and field-observed features of the structural domains (modified from Simonetti et al., 2020a); 1: folded micaschist of the External Zone (Bormes unit) cropping out to the W of the CF; 2: mylonite of the western side of the CF developed at the expense of staurolite-bearing micaschist (Bormes unit); 3: mylonite formed at the expense of paragneiss; 4: mylonitic paragneiss in the core of the CF; 5: mylonite at the expense of migmatite in the Internal Zone (La Garde-Freinet unit); 6: mylonite of the eastern limb of the CF affecting migmatite of the Internal Zone (La Garde-Freinet unit); 7: folded migmatite of the Internal Zone.

Schneider et al. (2014) hypothesised that the CF developed as a back-thrust with a top-to-the-E-SE sense of shear and subsequently it was reactivated as a normal fault.
Recently, kinematic vorticity analysis performed on sheared rocks of the CF has revealed transpressional deformation that occurred under general shear conditions with prevalent pure shear component (Simonetti et al., 2020a). According to Simonetti et al. (2020a), the CF progressively evolved into a transpressive shear zone during the retro-wedge building and, because of the dominant sub-horizontal pure shear component, it suffered verticalisation that allowed channelised vertical exhumation of the middle-lower crust of the Internal Zone.
Timing of deformation along the CF has been recently constrained thanks to *in-situ* microstructurally-constrained monazite U-Th-Pb petrochronology (Simonetti et al., 2020a). A complex monazite growth history during the tectono-metamorphic history was recognised. A first monazite generation with low-Y content, grew during

https://doi.org/10.3301/GFT.2022.04

prograde metamorphism, has been shown to occure between ~340 My and ~333 My (Oliot et al., 2015; Simonetti et al., 2020a) associated with the frontal collisional stage. A second group of monazites, with high-Y content, grew during retro-metamorphism and garnet breakdown linked to the activity of the CF at ~323 My (Simonetti et al., 2020a).

4. Itinerary

The field trip consists of eight stops (Fig. 5 and Table 1) located in southern France in the *Côte d'Azur* area, between the localities of Saint Tropez and Bormes. The place can be easily reached and the itinerary can be completed in one day but a sub-division of the excursion in two days is suggested. Most outcrops are located along the coast, so they are easily accessible.
A particular focus is given to the boundary between the Internal and External zones and on the km-scale transpressional shear zone known as the Cavalaire Fault (CF; Schneider et al., 2014; Oliot et al., 2015).
In the External Zone evidence of the D_1 collisional stage is well-preserved, as well as, the eastward increase of Barrovian metamorphism. In the first stop, the low-grade metasediments of the chlorite-chloritoid zone (stop 1) still preserve the original bedding surface (S_0) made of an alternation of coarse-grained layers and fine-grained layers. This early bedding is affected by F_1 folds with an associated S_1 axial plane foliation developed under low-grade metamorphic conditions (M_0 metamorphism, according to Schneider et al., 2014). In the second outcrop of the biotite-kyanite zone (stop 2), F_1 folds are rarely observed. Here, the S_1 foliation only occurs as internal foliation in staurolite, garnet and kyanite porphyroclasts suggesting that S_1 was completely transposed during the subsequent D_2 deformation after the collisional and crustal thickening stage. The Bormes orthogneiss and the associated kyanite-bearing micaschist of stop 2 are deformed by F_2 sheath folds. These folds are associated to an S_2 axial plane foliation with biotite and white mica, well-developed only in the kyanite-bearing micaschist. After collision and crustal thickening, several Authors recognised the onset of a syn-D_2 transpressional deformation regime (Bellot, 2005; Corsini and Rolland, 2009; Schneider et al., 2014; Oliot et al., 2015; Simonetti et al., 2020a). Transpressional deformation is responsible of the development of the CF along the boundary between Internal and External zones. CF non coaxial shearing affects rocks belonging to both zones. In mylonites formed at the expense of the External Zone (stop 3), syn-tectonic growth of biotite and white mica along the S_2 foliation in association with minerals such as staurolite testifies to amphibolite-facies metamorphism (M_2 metamorphic stage of Schneider et al., 2014) during shear deformation. Kinematic indicators, both at the meso and microscales,

https://doi.org/10.3301/GFT.2022.04

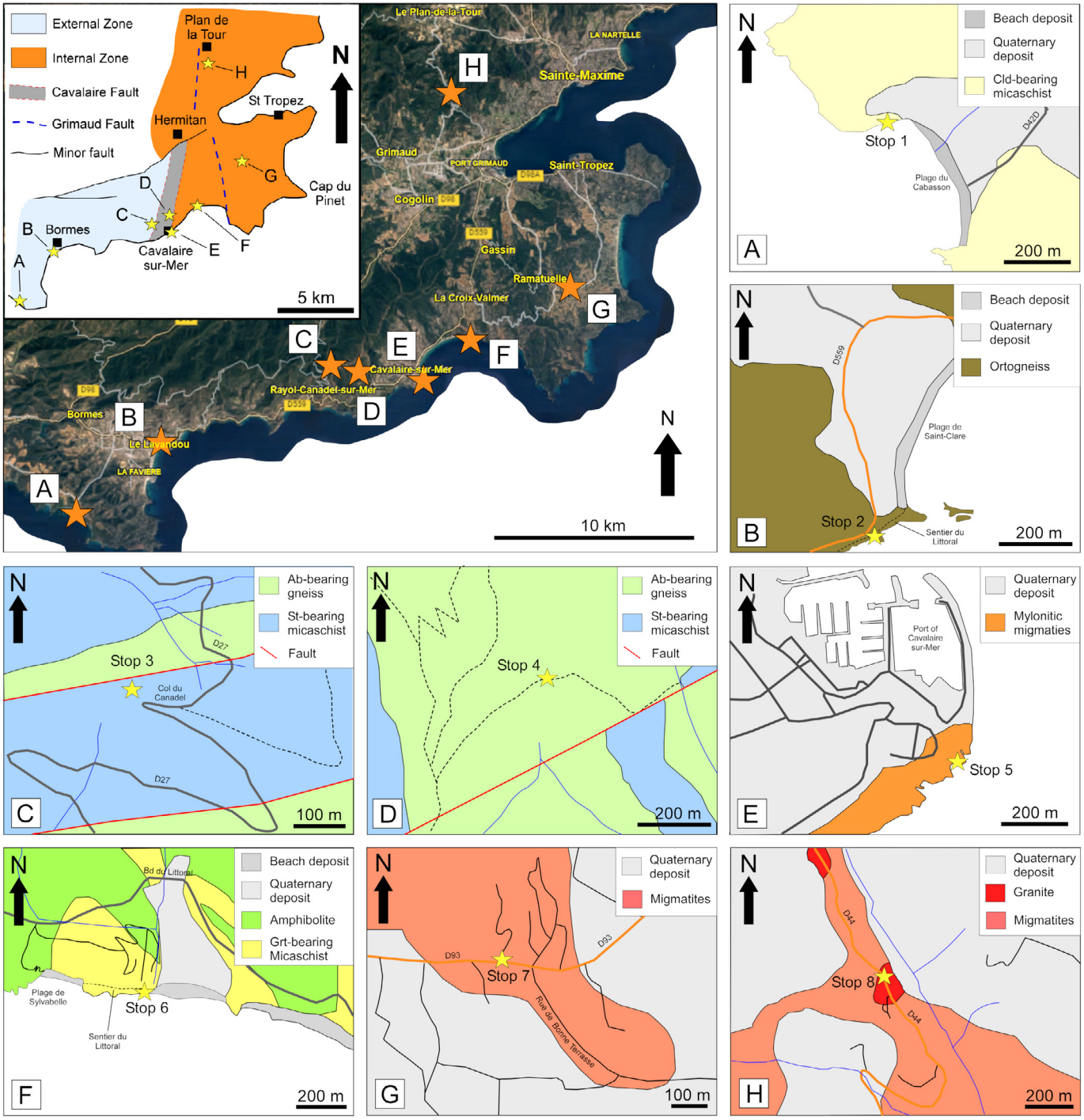

generally point to a top-to-the-NW sense of shear (stop 3 and stop 4). Because of the dominant pure shear component (Simonetti et al., 2020a), opposite kinematic indicators occur in some of the mylonites developed at the expense of the migmatite of the Internal Zone (stop 5).

Also the garnet-bearing micascist (stop 6) of the Internal Zone are affected by the CF and a top-to-the-NW sense of shear is recognised. In those outcrops a pure shear dominated transpression and a general flattening deformation are recognised.

During transpression, the Internal Zone was characterised by high-temperature metamorphism and

Fig. 5 - Geological sketch maps of the stops presented in the field trip (modified from Bordet and Gueirard, 1967; 1/50.000 geological maps of Saint Tropez-Cap Lardier and Hyères-Porquerolles, BRGM editions), satellite image is from Google Earth; the insert represents a schematic sketch of the main metamorphic zones of the Maures Massif. The stars in all figures represent the position of the stops.

https://doi.org/10.3301/GFT.2022.04

widespread partial melting (Schneider et al. 2014). These metamorphic conditions are in agreement with the occurrence of grain boundary migration as the main dynamic recrystallisation mechanism of quartz pointing to a deformation temperature higher than 500 °C. Such estimates are also confirmed by the data obtained from the quartz c-axis fabric opening angle thermometer.

Timing of shearing along the CF is well constrained thanks to monazite petrochronology data. A first group of monazite grew during prograde metamorphic conditions, linked to the first frontal collisional stage of the Variscan orogeny, between ~340 My and ~333 My, whereas a second group of monazites grew during the transpressional D_2 phase between ~327 My and ~323 My (Simonetti et al., 2020a).

The D_2 transpressional phase allowed the sub-vertical and channeled exhumation of the Internal Zone (Schneider et al., 2014; Gerbault et al, 2018; Simonetti et al., 2020a) thanks to the sub-horizontal pure shear component of deformation. During the D_2 phase partial melting with formation of migmatites (stop 7) occurred. D_2 deformation regime was responsible of the development of upright folds (stop 7) reflecting the presence of large-scale fold structures in the Internal Zone that are cored by late-orogenic granitoids intruding the migmatite (stop 8; Gerbault et al., 2018; Simonetti et al., 2020a).

The tectono-metamorphic features of the Maures Massif observed in this field trip are strikingly similar to those affecting the Variscan basement of northern Sardinia (Corsini and Rolland, 2009; Schneider et al., 2014; Carosi et al., 2020; Simonetti et al., 2020a). The Maures Massif and the northern Sardinia both show a low- to medium-grade complex and a migmatitic complex, with granitic intrusions, separated by a ductile transpressive shear zone active under nearly the same time span (late Carboniferous; Carosi et al., 2012; 2020; Simonetti et al., 2020a, 2020b, 2021b) and under comparable deformation and flow regime. These structural and geochronological observations support a model of the Corsica-Sardinia Block connected to southern France during late Carboniferous (Fig. 6a) and confirm that this sector of the belt was affected by transpressional deformation along the EVSZ (Fig. 6b).

https://doi.org/10.3301/GFT.2022.04

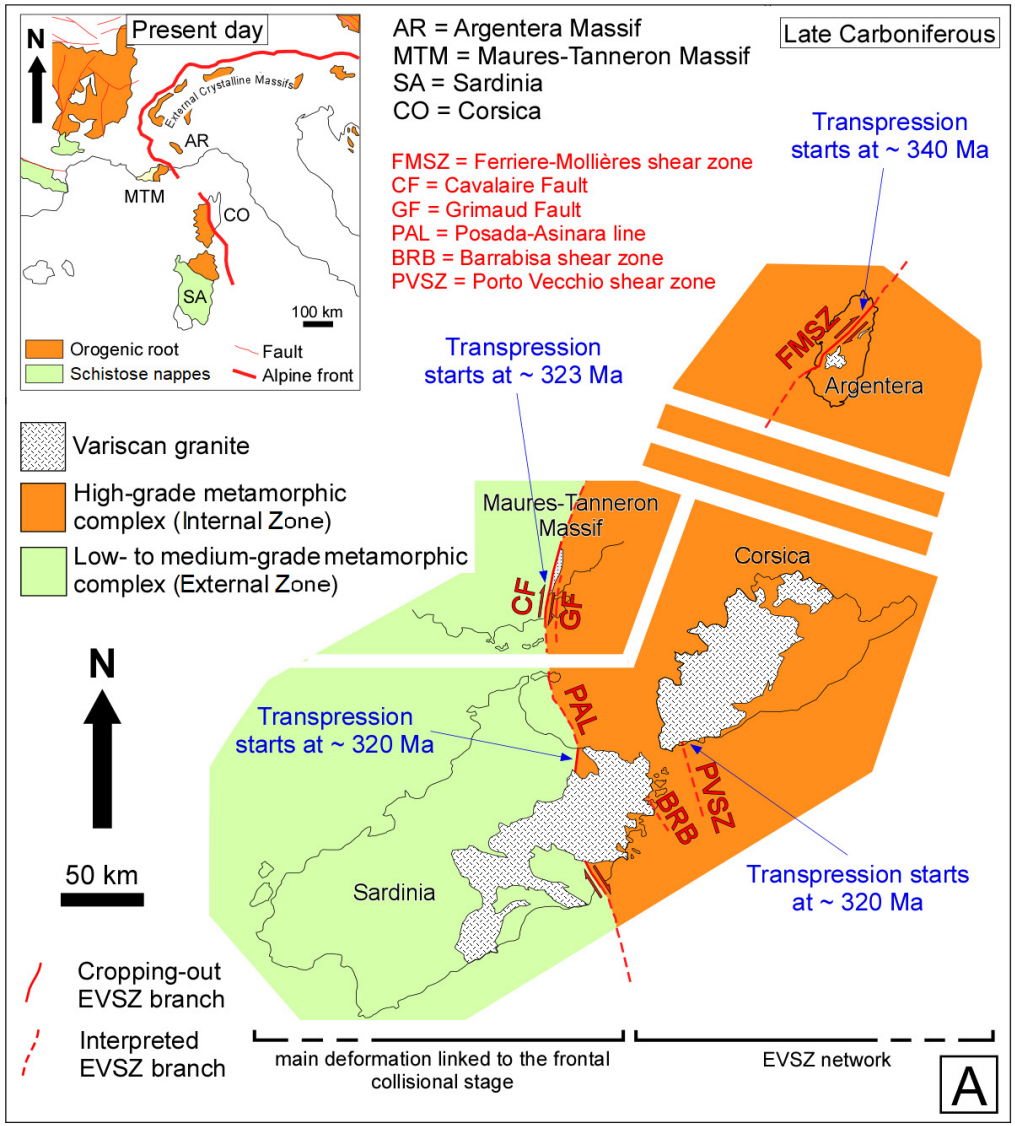

Fig. 6 - A) Structural sketch map of Mediterranean Variscan Europe (modified from Matte, 2001) showing present-day relations between Corsica-Sardinia Block, Maures-Tanneron Massif and Alpine External Crystalline Massifs and sketch of the possible late Carboniferous relationship between such sectors (modified after Simonetti et al., 2020a); timing of transpression is from Simonetti et al. (2018) for the FMSZ; Simonetti et al. (2020a) for the CF; Di Vincenzo et al. (2004) and Carosi et al. (2012) for the PAL and Giacomini et al. (2008) for the PVSZ; rotation of the Argentera Massif is from Collombet et al. (2002); B) schematic cross section of the EVSZ network with location of Sardinia, Maures Massif and Alpine External Crystalline Massifs (ECM).

https://doi.org/10.3301/GFT.2022.04

Stop 1 – External Zone, chloritoid-bearing micaschist at Cobasson village
(coord. 43°06'02.8"N; 006°19'20.6"E)

The first stop is located in the Cabasson area (Fig. 5a). It is possible to leave the car in the park of the Plage du Cabasson. The outcrop can be easily reached by walking a few minutes toward the northern termination of the beach (Fig. 7). This stop is representative of the low-grade External Zone (Fig. 4) and shows low-grade lower Palaeozoic metasediments belonging to the chlorite-chloritoid zone. The bedding, S_0, is defined by the alternation of coarse-grained decimetric layers consisting of quartz and biotite, and fine-grained layers rich in white mica, chlorite and few chloritoid crystals (Fig. 8a, 8b). The S_0 is deformed by F_1 folds (Fig. 8c) with NW-SE oriented sub-horizontal axes (Fig. 8d) and axial planes steeply dipping toward the S-SW. An S_1 axial plane foliation oriented NW-SE and steeply dipping toward the S-SW is present (Fig. 8d). On the S_1 foliation a mineral lineation L_1 consisting of elongated white mica and chloritoid moderately plunges toward the SE (Fig. 8d).

Fig. 7 - Outcrops of chloritoid-bearing micaschist of stop 1 located at the northern termination of the *Plage du Cabasson*.

The relationships between the S_0 and the S_1 can be observed both at the mesoscale (Fig. 8a) and at the microscale where it is also possible to recognise a selective development of the S_1 foliation in the fine-grained layers rich in phyllosilicates (Fig. 8e).

Stop 2 – External Zone, Bormes orthogneiss and kyanite-bearing micaschist
(coord. 43°08'21.0"N; 006°22'52.6"E)

From stop 1, driving east along the D42A road and then following the D559 for 9 km it is possible to reach the stop 2 at the Plage de Saint-Clair (Fig. 5b). The outcrop is located a few minutes walking along the *Sentier du Littoral* that runs southward along the beach (Fig. 5b).

https://doi.org/10.3301/GFT.2022.04

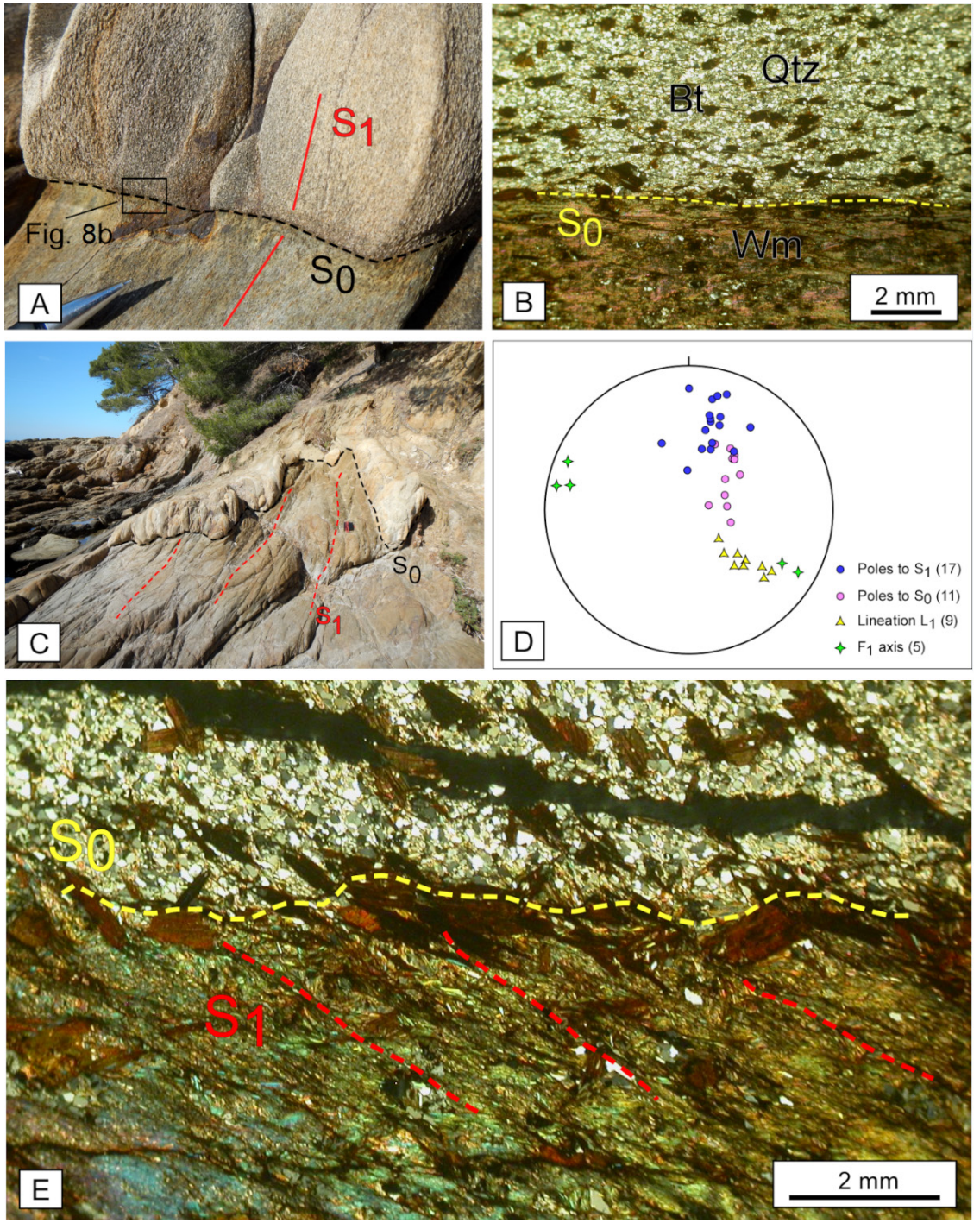

Fig. 8 - A) Low-grade lower Palaeozoic metasediments belonging to the chlorite-chloritoid zone showing relationship between the S_0 and the S_1 in correspondence of a F_1 fold hinge; B) appearance of the S_0 at the microscale, Bt = biotite; Qtz = quartz; Wm = white mica; C) F_1 folds deforming the S_0; D) Equal angle projection (lower hemisphere) of the main structural elements of the stop 1; E) relationships between the S_0 and the S_1 at the microscale (crossed nicols).

This stop is representative of the Bormes unit, within the biotite-kyanite zone of the External Zone. Here the Bormes unit is made of orthogneiss in contact with kyanite-bearing micaschist. The original contact is now transposed by an S_1 foliation (Fig. 9a) subsequently deformed by D_2. Micaschist is characterised by a biotite+white mica S_2 foliation wrapping around kyanite porphyroclasts (Fig. 9b). The two lithotypes are deformed by F_2 sheath folds (Fig. 9c) with NE-SW oriented axial planes (Fig. 9d) dipping at high angle toward the SE. F2 Axes plunge at high angle toward the S-SE, parallel to the L_2 object lineation, plunging at high angle toward the SE (Fig. 9d). The S_2 foliation in the micaschist is oriented NE-SW and dips at high angle toward the SE. S_2 is parallel to the axial plane of the sheath folds (Fig. 9d). The presence of two foliations testifies to a polyphase deformation and in some places the relationship between the two deformation phases is clearly recognisable thanks to the occurrence of type-3

https://doi.org/10.3301/GFT.2022.04

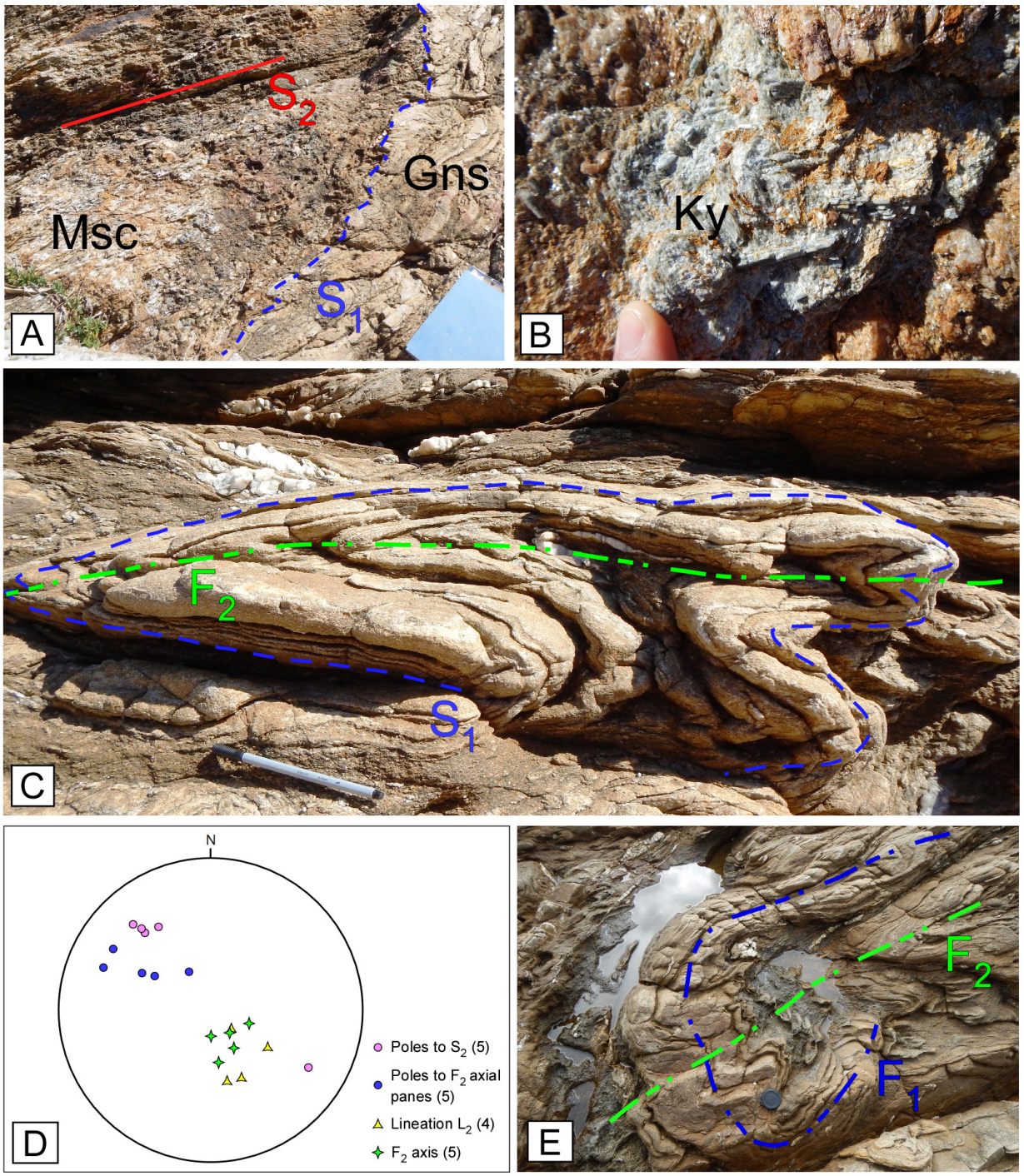

Fig. 9 - A) Orthogneiss (Gns) in contact with kyanite-bearing micaschist (Msc) through a deformed S_1 foliation, the micaschist shows S_2 foliation; B) kyanite porphyroclast (Ky) within the kyanite-bearing micaschist; C) F_2 sheath fold in Bormes orthogneiss; D) equal angle projection (lower hemisphere) of the main structural elements of the stop 2; E) type-3 fold interference pattern between F_1 and F_2 folds.

fold interference pattern (Fig. 9e; Ramsay and Huber, 1987).

D_1 deformation of the Bormes orthogneiss was dated by Moussavou (1998) between 345 ± 3 My and 339 ± 16 My (TIMS, thermal ionization mass spectrometry). Due to the syn-tectonic growth of both garnet and kyanite, D_1 was interpreted as linked to the crustal thickening phase (the first stage of the Variscan orogeny; Oliot et al., 2015), whereas the D_2 deformation is linked to the post-collisional phase of the Variscan orogeny as widely documented both in the Maures Massif (Schneider et al., 2014) and in northern Sardinia (Carosi and Palmeri, 2002; Carosi et al., 2020).

https://doi.org/10.3301/GFT.2022.04

Stop 3 – Transition Zone, staurolite-bearing micaschist of the Cavalaire Fault at Col du Canadel (coord. 43°10'09.1"N; 006°28'29.0"E)

Stop 3 is located at the Col du Canadel (Fig. 5c) that, starting from stop 2, can be reached following the D559 road and then the D27 road towards the E for 13 km. At this stop rocks belonging to the Transition Zone (Fig. 10) and the first evidence of deformation related to the CF activity occurs.
Sheared staurolite-kyanite and staurolite-bearing micaschist, belonging to the Bormes unit (Fig. 10), shows a S_2 biotite + white mica mylonitic foliation, oriented NE-SW and dipping to the NW at moderate or low angle (Fig. 11a), with a mineral lineation L_2 defined by staurolite plunging at low angle to the NW (Fig. 11a). Shear planes dip towards W-NW at variable angles in the 14° and 53° range. Asymmetric strain fringes of quartz around staurolite porphyroclasts (Fig. 11b), S-C fabric and asymmetric quartz and feldspar aggregates indicate a top-to-the-NW sense of shear. The main foliation is subsequently deformed by a steeply dipping NW-SE oriented crenulation cleavage S_3 (Fig. 11c) with microfold axes plunging toward the NW at low angle (Fig. 11a). S_3 is occasionally associated with dynamic recrystallisation of chlorite.
At the microscale the mylonitic foliation is an anastomosing spaced foliation wrapping around kyanite, staurolite and garnet porphyroclasts that, in some cases, contain an internal foliation mainly composed of elongated quartz inclusions. The internal foliation in the porphyroclasts is generally not continuous with the external foliation (Fig. 11d). However, in some staurolite crystals, an internal foliation at the grain rims is concordant with the external one (Fig. 11e) so this implies that staurolite is not always a porphyroclast, but in some cases it is a syn-tectonic porphyroblast. These observations support the interpretation that staurolite growth predates, and is locally synchronous to, the development of the mylonitic foliation.
Lobate and ameboid quartz grain boundaries (Fig. 11f) suggest dynamic recrystallisation by grain boundary migration pointing to deformation temperatures above 500-550 °C (Law, 2014).
In-situ microstructurally constrained monazite U-Th-Pb petrochronology (Fig. 12a, 12b) was recently performed on those rocks by Simonetti et al. (2020a). Microstructural position, texture, zoning, and chemical analyses, highlight a complex history of monazite growth during the tectono-metamorphic history. A first group of monazites, characterised by a low-Y content, grew during prograde metamorphic conditions associated with the frontal collisional stage, whereas a second group, characterised by high-Y content, grew during retro-metamorphism and garnet breakdown linked to the activity of the CF. Timing of prograde metamorphism ranges between ~340 My and ~333 My (Fig. 12c; Oliot et al., 2015; Simonetti et al., 2020a). Those ages are preserved in the low Y

https://doi.org/10.3301/GFT.2022.04

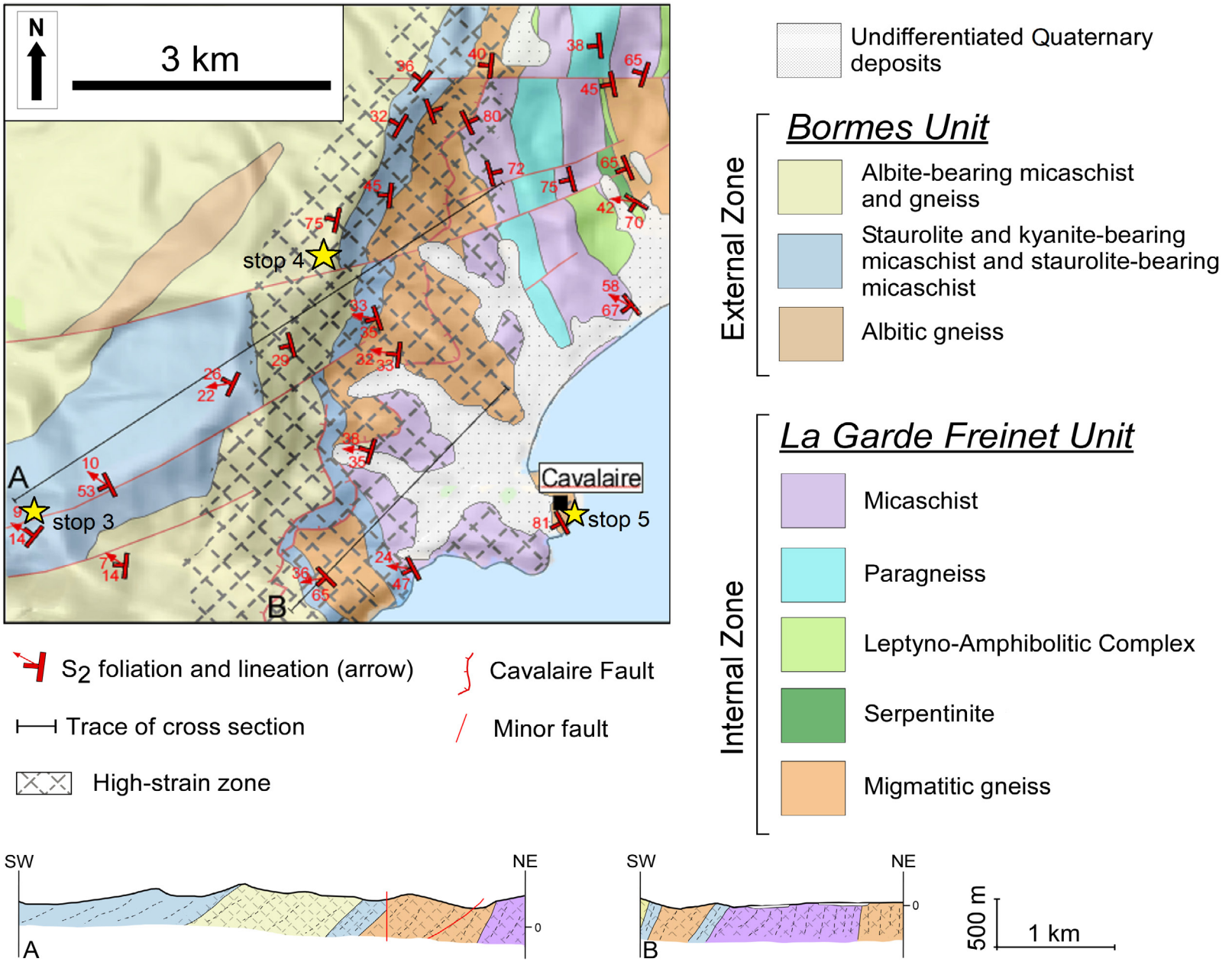

Fig. 10 - Geological sketch map and cross sections of the Transition Zone and of the Cavalaire Fault (modified from Simonetti et al., 2020a).

https://doi.org/10.3301/GFT.2022.04

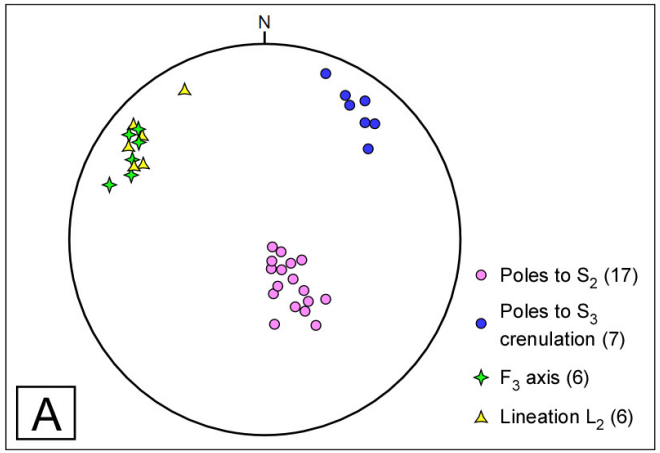

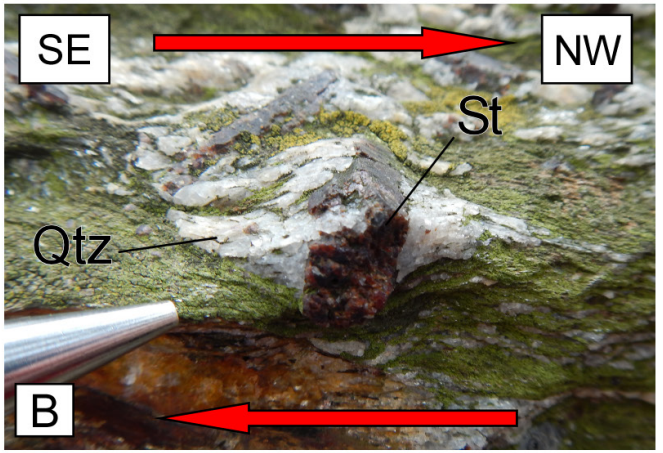

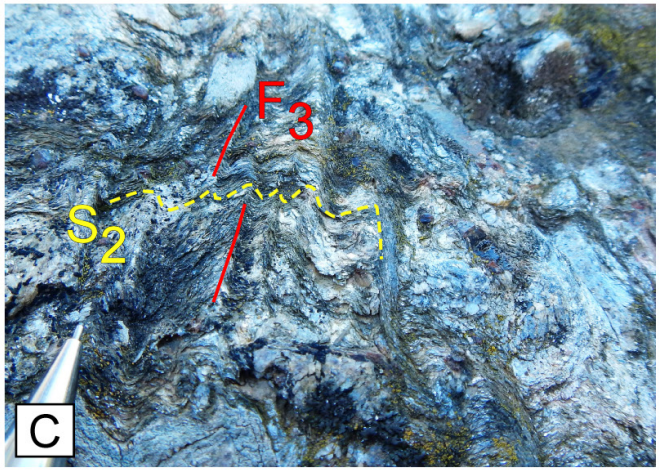

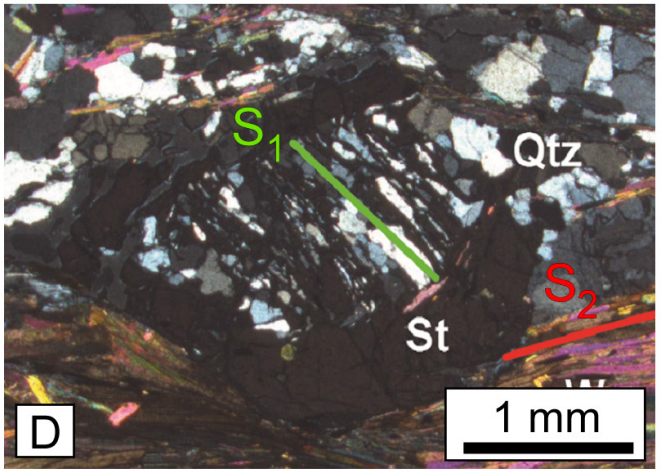

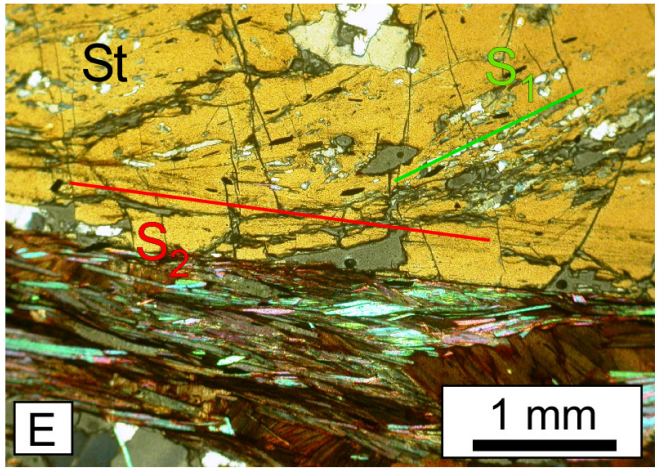

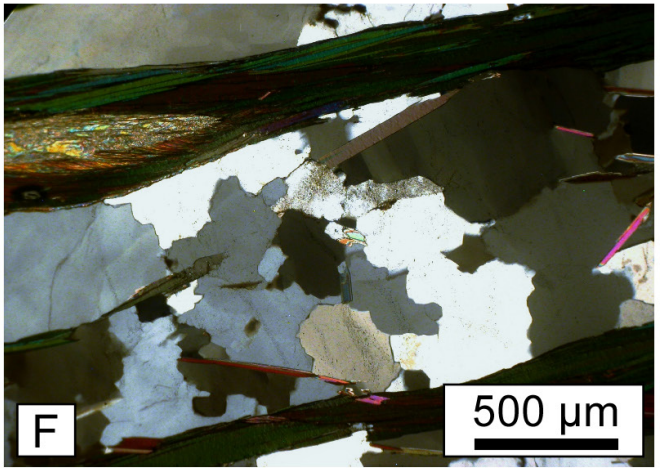

Fig. 11 - A) Equal angle projection (lower hemisphere) of the main structural elements of the stop 3; B) top-to-the-NW sense of shear highlighted by asymmetric quartz strain fringes around a staurolite porphyroclast in staurolite-bearing micaschist (modified from Simonetti et al., 2020a); C) crenulation cleavage S_3 at the outcrop scale; D) staurolite porphyroclast in kyanite-bearing micaschist with an internal foliation S_1 defined by quartz + white mica; the porphyroclast is wrapped by the external foliation S_2 defined by quartz + white mica (crossed nicols; modified from Simonetti et al., 2020a); E) staurolite showing two stages of growth: an inter-tectonic core with an internal foliation S_1 and a syn-tectonic rim with an internal foliation S_2 in continuity with the external one (crossed nicols); F) lobate and ameboid quartz grain boundaries indicative of dynamic recrystallisation by grain boundary migration; Qtz = quartz; St = staurolite.

cores of monazite grains or in grains included in porphyroclasts. Younger ages of ~323 My, related to the shearing, were obtained from high-Y rims of monazite grains along the mylonitic foliation (Fig. 12c; Simonetti et al., 2020a).

https://doi.org/10.3301/GFT.2022.04

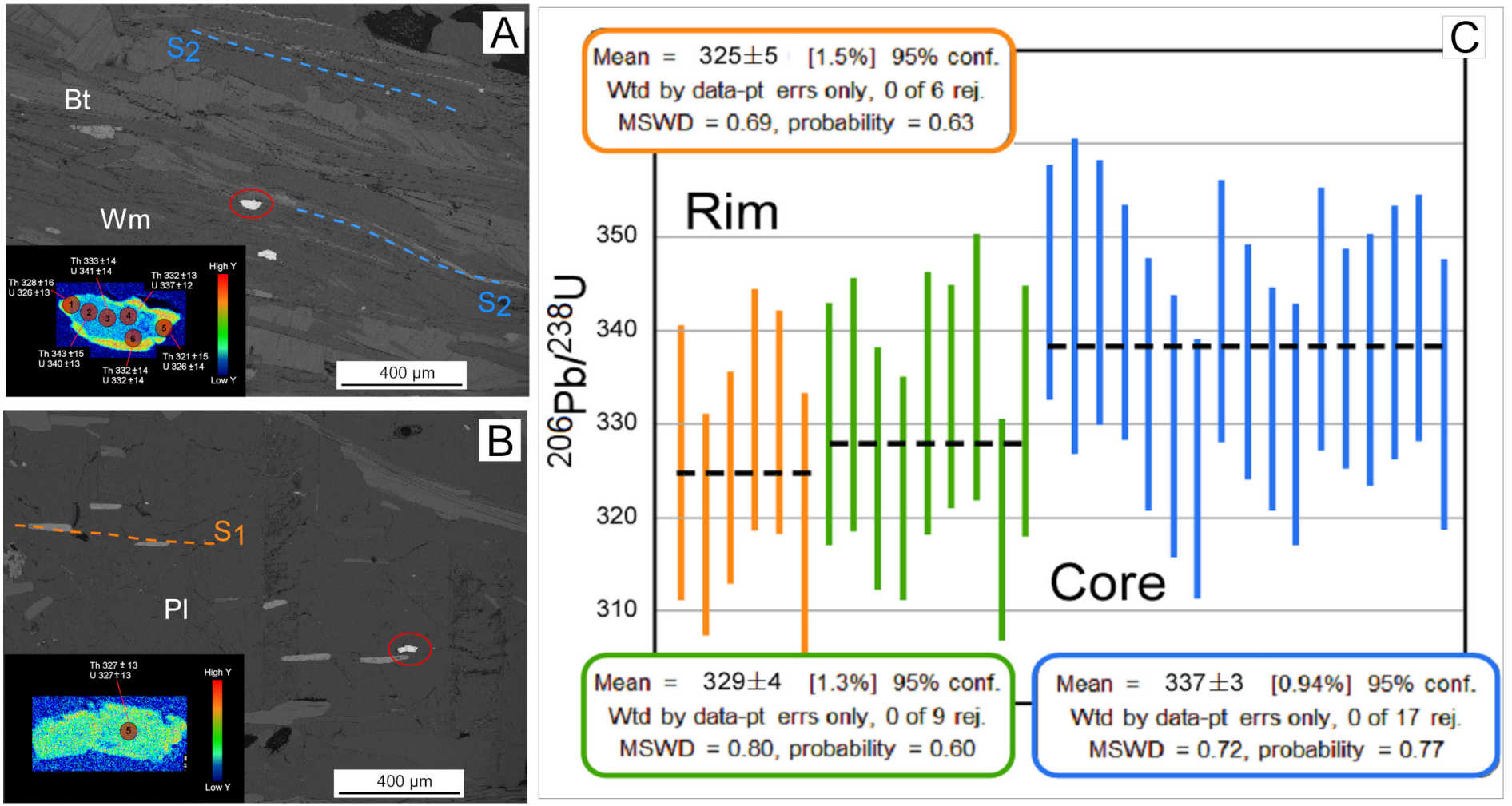

Fig. 12 - Examples of textural position and zoning of monazite grains selected for *in situ* dating by Simonetti et al. (2020a) and obtained results for a kyanite-bearing micaschist: A) BSE image of a monazite grain located along the S_2 foliation and relavite Y compositional map; B) BSE image and relavite Y compositional map of a monazite grain located included in a plagioclase porhyroclast along the relict S_1 foliation; C) distribution of 207-corrected $^{206}Pb/^{238}U$ ages obtained from a kyanite-bearing micaschist; data are grouped according to the position of the spot within the grain and colors of the bars are organised according to the Y content: blue = low-Y domain in the core of the grain; green = medium-Y domain in the core of the grain or in an intermediate position between core and rim (mantle); orange = high-Y domain in the rim of the grain. MSWD = mean square weighted deviates (modified from Simonetti et al., 2020a); Bt = biotite, Wm = white mica, Pl = plagioclase.

https://doi.org/10.3301/GFT.2022.04

Stop 4 – Transition Zone, mylonitic gneiss of the Cavalaire Fault
(coord. 43°11'11.0"N; 006°30'08.5"E)

This stop is located along a dirt road (called *Route Forestière de Pradels*) that connects the Col du Canadel with the village of Cavalaire sur-Mer (Fig. 5d) nearly 4 km after stop 3.
Here, the mylonitic gneiss (Fig. 13) in the core of the CF (Fig. 10) can be observed. A N-S oriented penetrative S_2 mylonitic foliation steeply dipping to the W with a mineral lineation plunging at medium angle to the W-NW (Fig. 14a) can be observed. The sense of shear, highlighted by S-C and S-C' fabric, is top-to-the-NW (Fig. 14b). In some sectors a sub-vertical NW-SE oriented S_3 crenulation cleavage (Fig. 14a), overprinting the mylonitic foliation, is present.
At the microscale, quartz grains show lobate grain boundaries and pinning microstructures indicative of dynamic recrystallisation by grain boundary migration (Fig. 14c) under temperature range between 500° C and 700° C. Quartz fabric opening angle thermometer (Faleiros et al., 2016) confirms this temperature by providing a data beetween ~550 °C and ~613 °C (Fig. 14c; Simonetti et al, 2021a). Kinematic vorticity analysis performed using the C' shear band method (Fig. 14d; Kurz and

Fig. 13 - Appearance of mylonitic gneiss in the core of the CF at the outcrop-scale.

https://doi.org/10.3301/GFT.2022.04

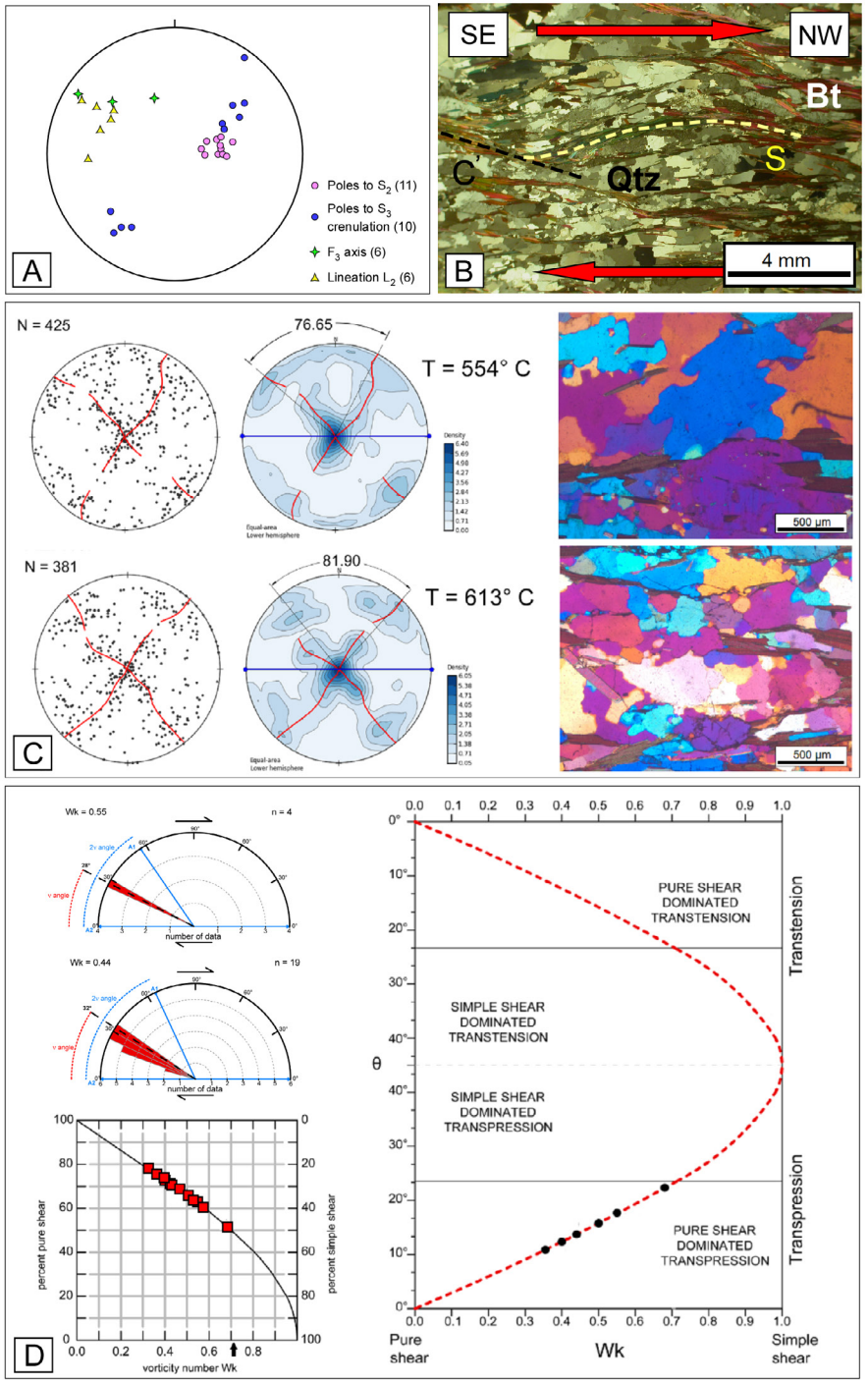

Fig. 14 - A) Equal angle projection (lower hemisphere) of main structural elements of the stop 4; B) S-C' fabric showing a top-to-the-NW sense of shear (crossed nicols); C) optically measured quartz c-axis in mylonitic samples from stop 4, all pole figures are oriented perpendicular to the foliation and parallel to the lineation. Blue line is the main foliation and blue dots are the mineral lineation. Fabric opening angle and the obtained temperature is reported as well as an example of the observed quartz microstructure (modified from Simonetti et al., 2021); D) kinematic vorticity analysis performed with the C' shear band method and obtained results (modified from Simonetti et al., 2020a).

Northrup, 2008) on samples from this outcrop revealed a non coaxial transpressional deformation. Obtained vorticity numbers range from 0.40 to 0.68, with a mean of 0.47 and a mode of 0.44. These data are indicative of a flow regime characterised by an important contribution of pure shear ranging between 52% and 66% (Fig. 14d).
Monazite U-Th-Pb petrochronology revealed a deformation age of ~327 My obtained from high-Y rims of grains located along the mylonitic foliation (Fig. 15). Low-Y cores of such grains, provided older ages of ~335 My, that are in good agreement with the timing of the prograde metamorphism linked to the collisional stage (Fig. 15; Oliot et al., 2015; Simonetti et al., 2020a).

Stop 5 – Transition Zone, mylonitic migmatite of the Cavalaire Fault at Cavalaire sur-Mer

(coord. 43°10'07.8"N; 006°32'23.4"E)

This stop is located close to the port of Cavalaire sur-Mer (Fig. 5e). The outcrop can be reached by walking south along the artificial cliff.

https://doi.org/10.3301/GFT.2022.04

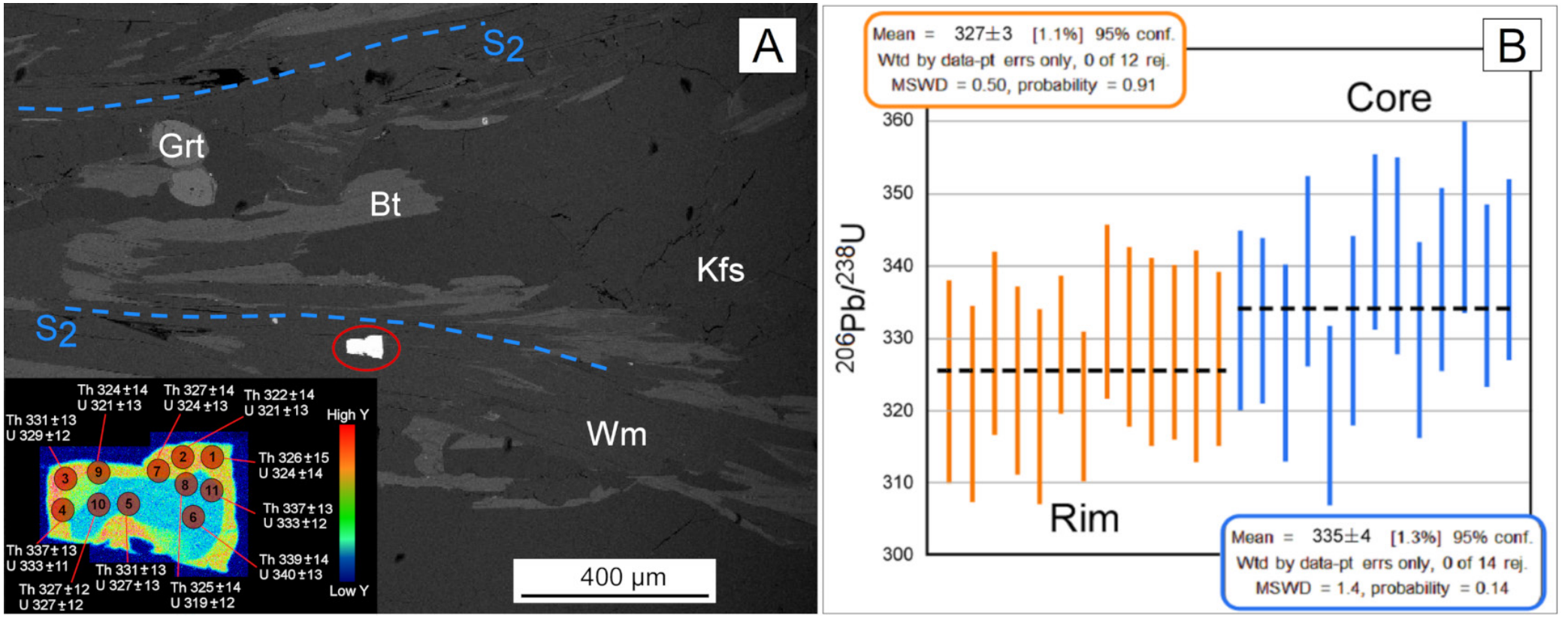

Fig. 15 - A) Example of microstructural position and zoning of a monazite grain, located along the S_2 foliation, selected for *in situ* dating by Simonetti et al. (2020a) within the mylonitic gneiss of stop 4; B) distribution of 207-corrected $^{206}Pb/^{238}U$ ages obtained from a mylonitic gneiss; data are grouped according to the position of the spot within the grain and colors of the bars are organised according to the Y content: blue = low-Y domain in the core of the grain; orange = high-Y domain in the rim of the grain. MSWD = mean square weighted deviates (modified from Simonetti et al., 2020a); Bt = biotite, Grt = garnet, Kfs = k-feldspar, Wm = white mica.

La Garde-Freinet unit, located to the east of the mylonitic gneiss of stop 4 (Fig. 10), is affected by non-coaxial deformation linked to the activity of the CF. Sheared migmatite of the Internal Zone belonging to this unit shows a NW-SE oriented sub-vertical S_2 mylonitic foliation (Figs. 16 and 17a) defined by biotite and sillimanite. An object lineation L_2 plunging toward W-NW at medium angle is also present (Fig. 16a). Both dextral and sinistral kinematic indicators occur (Fig. 17b) such as σ and δ mantled porphyroclasts, shear-band boudins and S-C fabric.

https://doi.org/10.3301/GFT.2022.04

Fig. 16 - Outcrop of mylonitic migmatite of the Cavalaire Fault at the port of Cavalaire sur-Mer (stop 5).

At the microscale, quartz grains have lobate grain boundaries (Fig. 17c) and pinning microstructures (Fig. 17d) suggesting dynamic recrystallisation by grain boundary migration under a temperature range between 500° C and 700° C. In agreement, quartz c-axis fabric analysis (Fig. 17e) and the opening angle thermometer gives temperatures of ~640 °C (Simonetti et al., 2021a).
Kinematic vorticity analysis performed applying the C' shear band method (Fig. 14d) revealed a transpressional deformation characterised by an important contribution of pure shear up to ~70% (Fig. 14c). The prevalent pure shear component is in good agreement with both the occurrence of opposite kinematic indicators and with the geometry of the quartz c-axis fabric suggesting general flattening strain conditions (Schmid and Casey, 1986).

https://doi.org/10.3301/GFT.2022.04

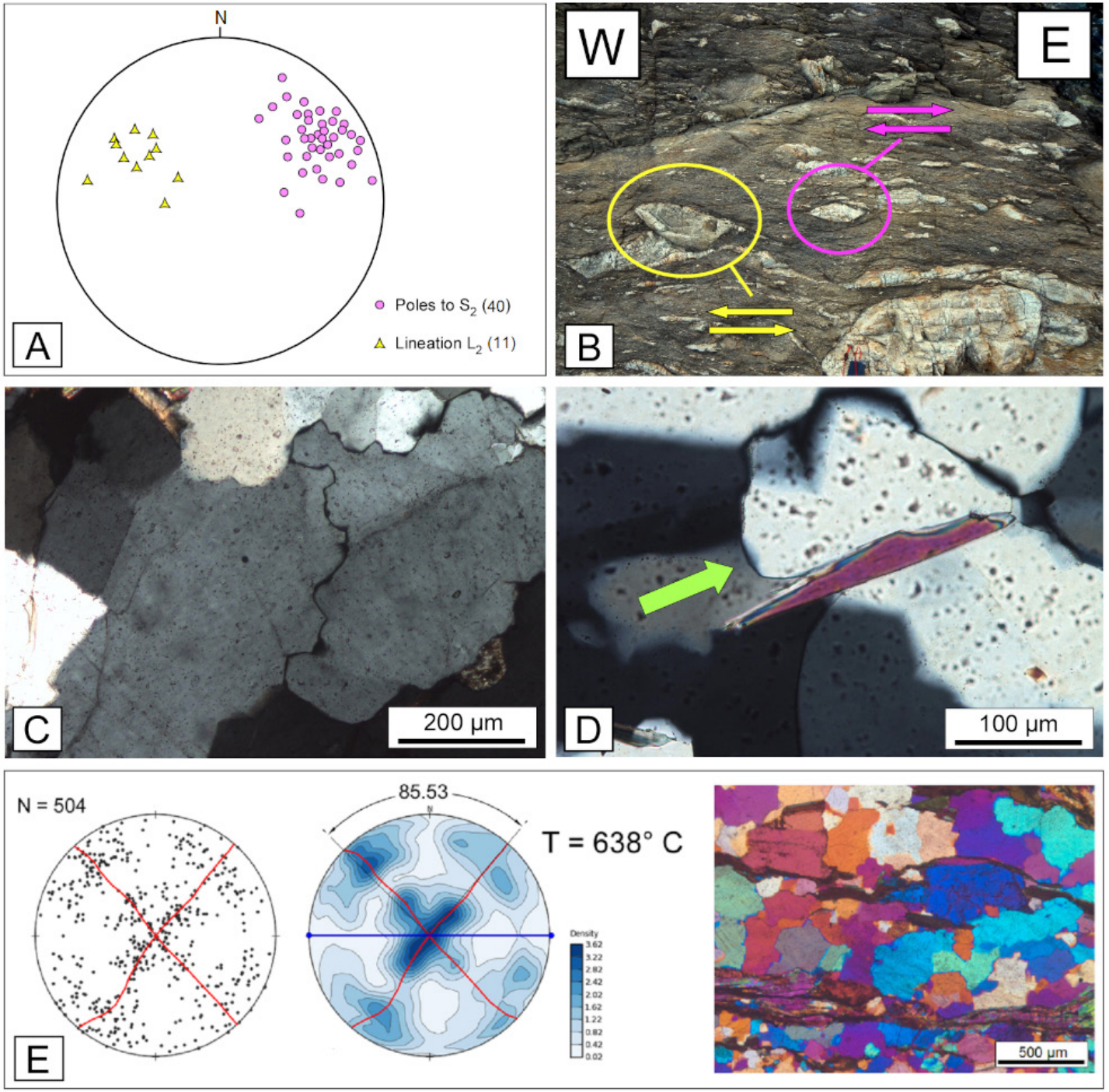

Fig. 17 - Equal angle projection (lower hemisphere) of the main structural elements of the stop 5; B) sheared migmatite showing both dextral and sinistral sense of shear; C) quartz showing lobate and ameboid grain boundary indicative of recrystallisation by graing boundary migration; D) pinning microstructure (green arrow); E) optically measured quartz c-axis in mylonitic samples from stop 5, all pole figures are oriented perpendicular to the foliation and parallel to the lineation. Blue line is the main foliation and blue dots are the mineral lineation. Fabric opening angle and the obtained temperature is reported as well as an example of the observed quartz microstructure (modified from Simonetti et al., 2021).

https://doi.org/10.3301/GFT.2022.04

Stop 6 – Internal Zone, mylonitic garnet-bearing micaschist
(coord. 43°11'11.2"N; 006°35'11.5"E)

This stop is located between the *Plage de Sylvabelle* and the *Plage d'Héraclée* along the *Sentier du Littoral* that connects the two localities (Fig. 5f). The car can be left at the parking of the *Plage de Sylvabelle*. Then follow on foot the *Sentier du Littoral* up to the outcrops that separate the two beaches (Figs. 18 and 19). Here garnet-bearing micaschist (Figs. 18 and 20a), interpreted as metavolcanic rocks of transitional to tholeiitic affinity, crops out. These rocks are also known in the literature as "alkaline leptyno-amphibolitic complex" (Schneider et al., 2014), they belong to the La Garde-Freinet unit (Figs. 3 and 18) and are part of the Internal Zone (Fig. 4). Micaschist is deformed together with amphibolite layers by F_2 folds (Figs. 18, 20b and 21) with subvertical axial planes and subvertical axis (Fig. 19a). An older S_1 foliation is preserved in the amphibolite. Axial plane S_2 foliation is well developed in the micaschist, it strikes N-S (Fig. 22a) and a subvertical mineral lineation, L_2, punging toward the S is present (Fig. 22a). S_2 is a spaced schistosity with sharp and parallel cleavage domains defined by biotite + white mica. At the microscale is possible to observe that garnet porphyroclasts show an internal foliation, marked by inclusions of elongated quartz, oriented at a high-angle with respect to the external foliation suggesting an inter-tectonic growth (between the D_1 and D_2) of such mineral. Quartz shows lobate grain boundaries indicative of dynamic recrystallisation by grain boundary migration.
Rocks in this outcrop show evidence of non-coaxial deformation linked

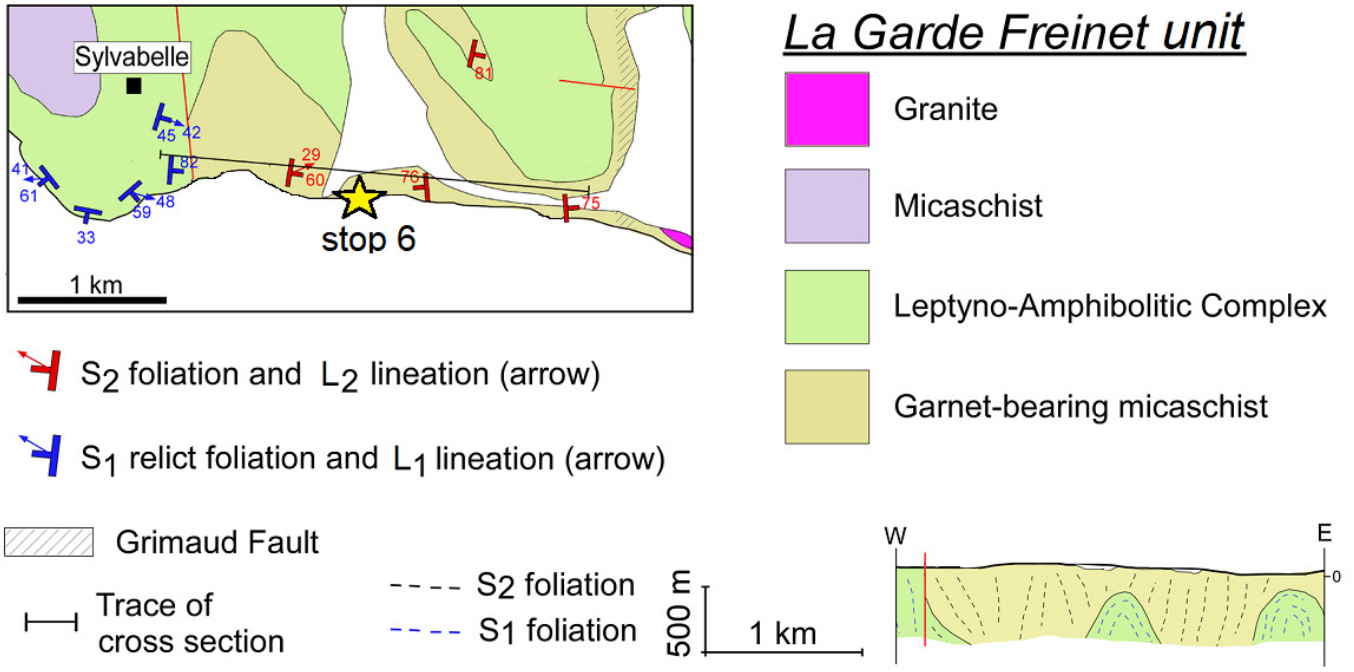

Fig. 18 - Geological sketch map and cross section of the area of stop 6 (modified from Simonetti et al., 2020a).

https://doi.org/10.3301/GFT.2022.04

Fig. 19 - Outcrops of garnet-bearing micaschist separating the *Plage de Sylvabelle* and the *Plage d'Héraclée* along the *Sentier du Littoral* (stop 6).

https://doi.org/10.3301/GFT.2022.04

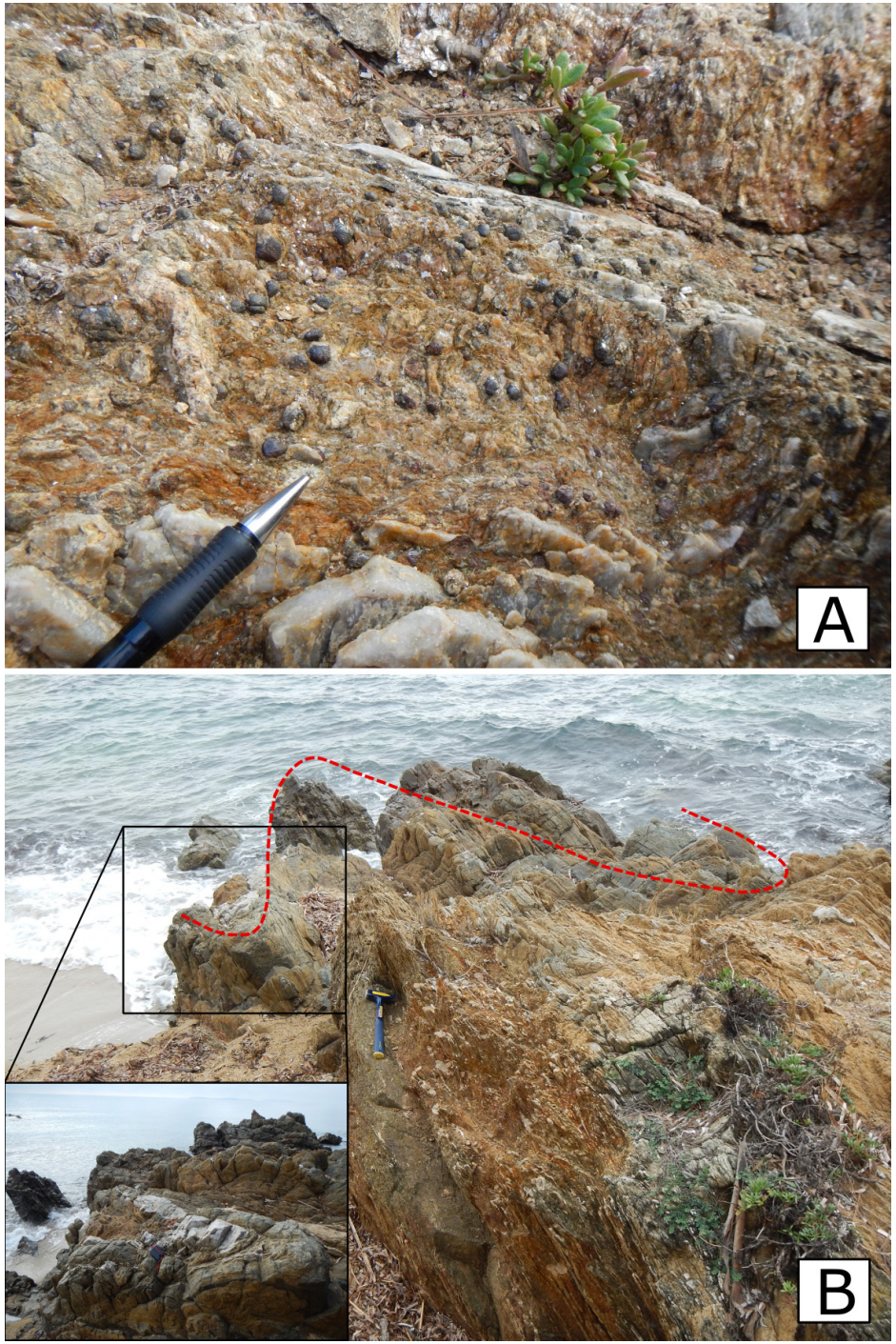

Fig. 20 - A) Garnet-bearing micaschist at the outcrop-scale; B) micaschist deformed together with amphibolite layers by F_2 folds (red dashed line) with a subvertical axial planes and subvertical fold axis.

to the activity of the CF such as rotated porphyroclasts, S-C and S-C' fabric. Kinematic indicators, recognisable both at the microscale and at the mesoscale, point to a top-to-the-NNW sense of shear (Fig. 22b).

Kinematic vorticity (Wk) and finite strain were analysed by Simonetti et al. (2020a). The study revealed a pure shear-dominated transpressional regime (Fig. 14d) and a general flattening strain (Fig. 23). Using Wk (vorticity number) values and finite strain estimates from samples collected in this outcrop (following Wallis et al., 1993; Law et al., 2004; Law, 2010), a stretching amount parallel to the transport direction of 41% and 40% were obtained.

Monazite U-Th-Pb petrochronology, recently performed by Simonetti et al. (2020a), allowed to obtain ages from one grain included in garnet porphyroclast and two grains included in syn-kinematic white mica on the S_2. The analysis revealed ages of ~335 My obtained from rims and of ~340 My from the core of the grains. Little difference in the absolute timing of high- and low-Y cores (340 ± 4 My and 341 ± 3 My, respectively) was detected and reflects a rapid phase of prograde metamorphism during collision.

https://doi.org/10.3301/GFT.2022.04

Fig. 21 - Micaschist deformed by an F_2 fold (red dashed line) with subvertical axial plane (stop 6)

https://doi.org/10.3301/GFT.2022.04

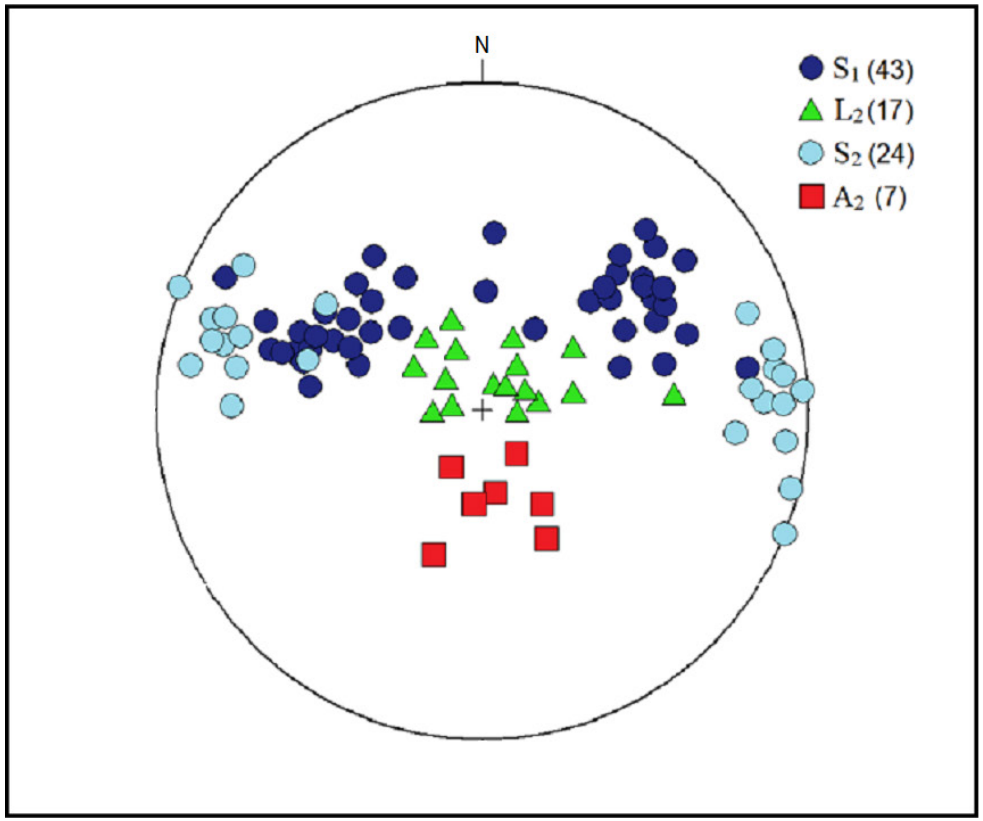

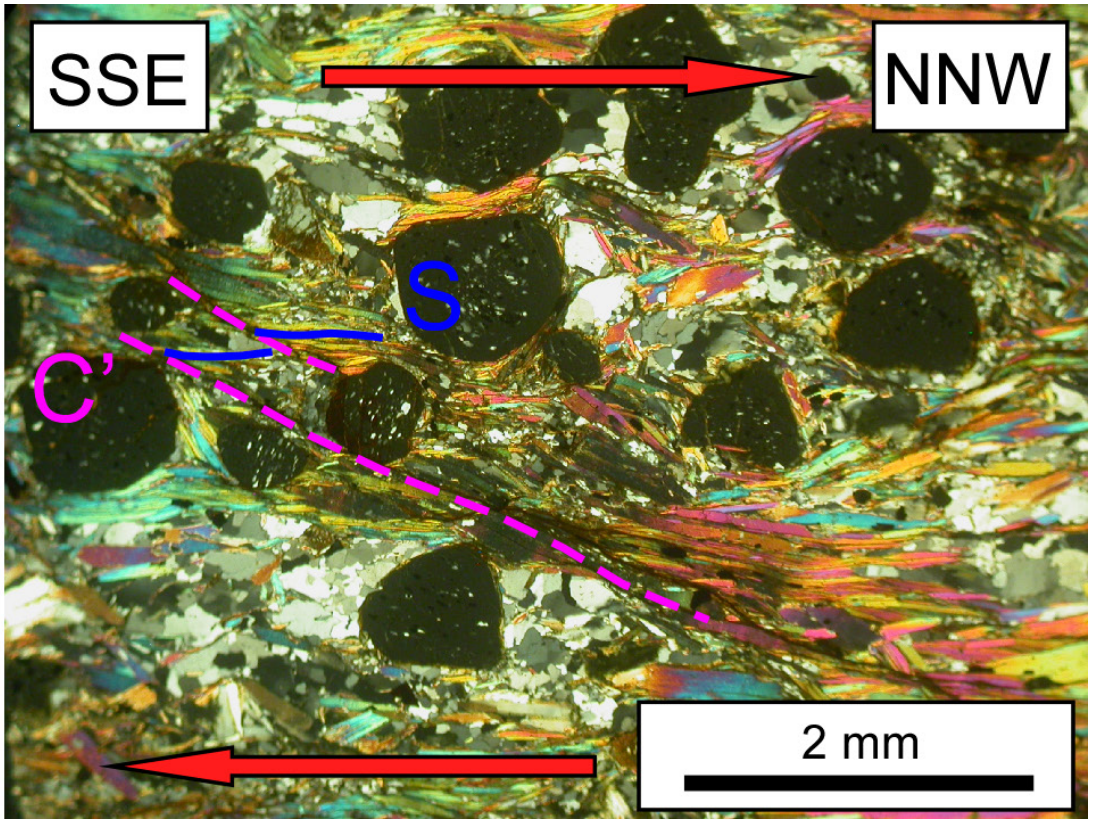

Fig. 22 - A) Equal angle projection (lower hemisphere) of the main structural elements of the stop 6 (modified from Simonetti et al., 2020a); B) garnet-bearing micaschist at the microscale showing S-C' fabric indicatunitive of a dextral top-to-the-NNW sense of shear.

https://doi.org/10.3301/GFT.2022.04

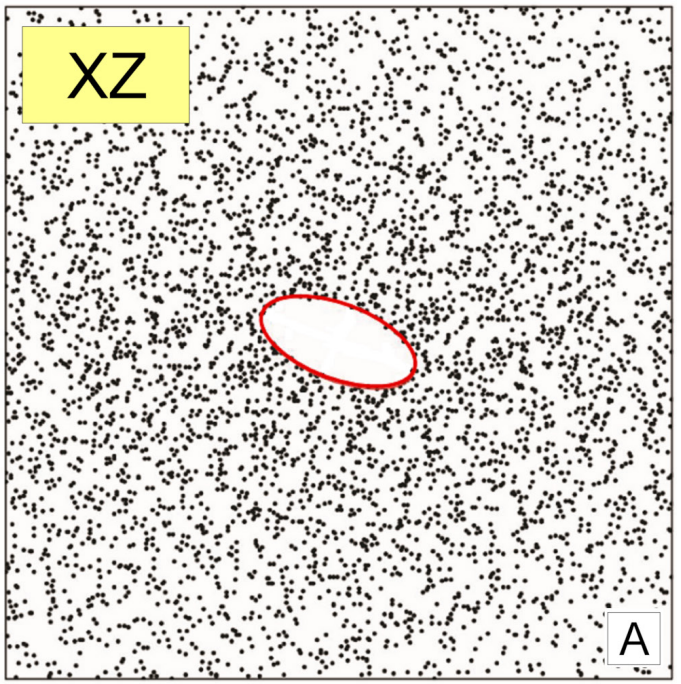

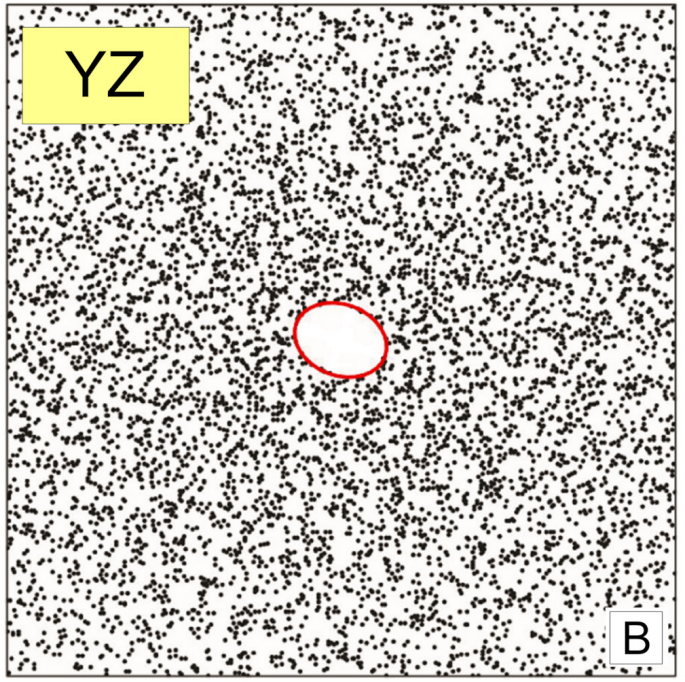

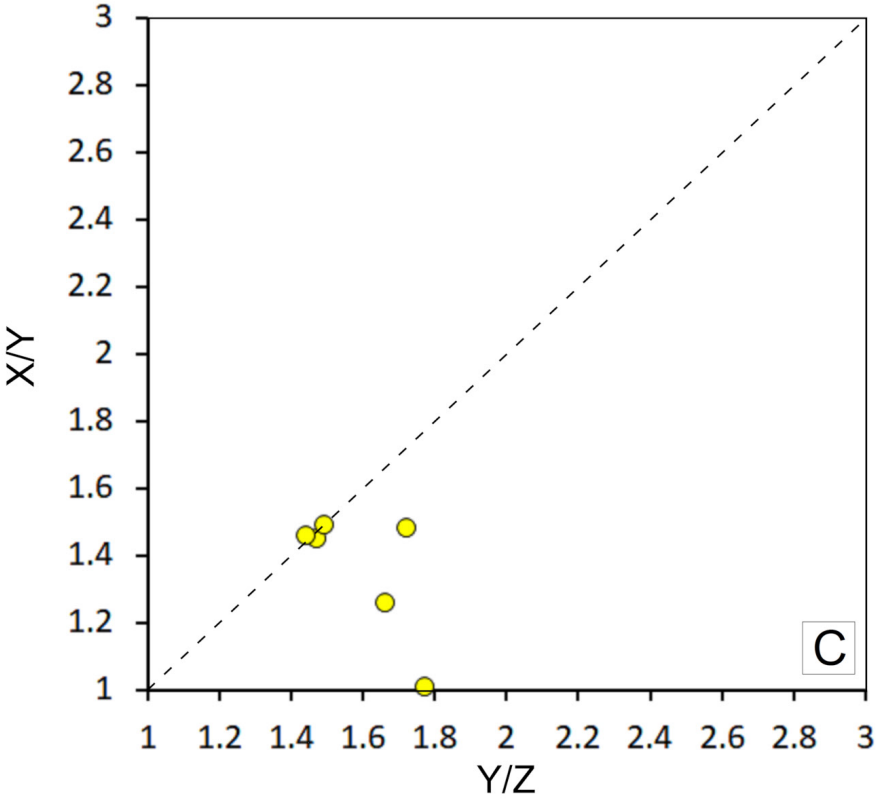

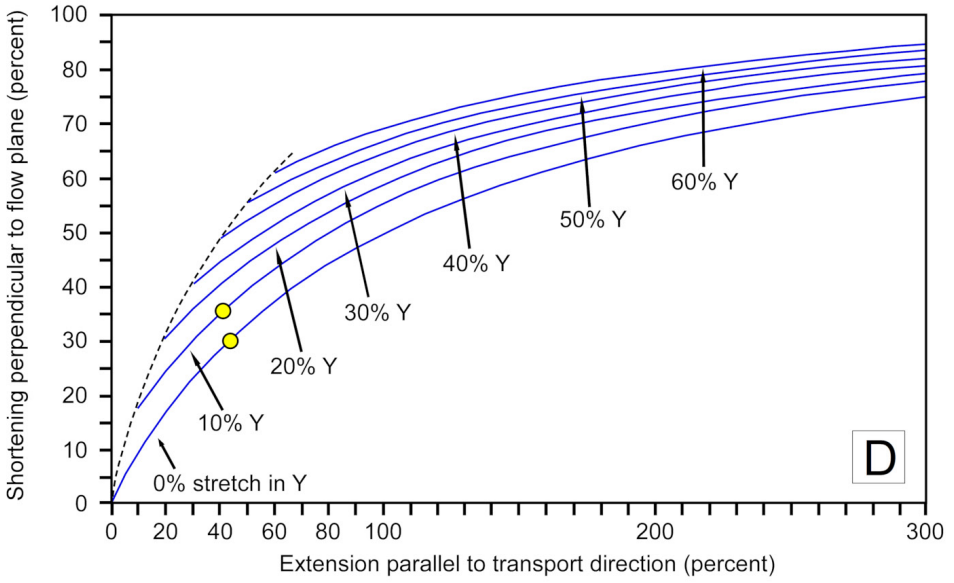

Fig. 23 - Results of finite strain analysis: A) example of Fry graph, based on the center-to-center method, for the XZ section; B) example of Fry graph, based on the center-to-center method, for the YZ section; C) Flinn diagram showing the position in the apparent flattening field of the studied samples (modified from Simonetti et al., 2020a); D) curves representing the shortening perpendicular to flow plane versus extension in transport direction for general flattening with stretch along Y between 0-60% (modified from Law, 2010 and Simonetti et al., 2020a).

https://doi.org/10.3301/GFT.2022.04

Stop 7 – Internal Zone, unsheared migmatite
(coord. 43°12’41.5’’N; 006°38’09.5’’E)

From stop 6, by car, we move northward. We reach the D93 road and we drive along it toward the NE for nearly 12 km. The outcrop is located on the left, in correspondence of a crossroad between the D93 and a small private nameless road (Fig. 5g). The car can be parked along the road near the outcrop. Here, migmatite of the Internal Zone, belonging to the La Garde-Freinet unit (Fig. 3), are exposed. Migmatites of the Maures Massif derived from both orthogneiss and paragneiss. They contain amphibolitised eclogite lenses (Le Marrec, 1976; Maquil, 1976; Crévola, 1977; Vauchez, 1987) recording early HP metamorphism that, however, is not preserved in the surrounding rocks. Such lenses are interpreted as the evidence of a dismembered suture zone (Schneider et al., 2014; Oliot et al., 2015). Orthogneiss and paragneiss have experienced partial melting, during the late Visean (zircon U-Pb, 334 ± 3 My; Lancelot et al., 1998), linked to their exhumation stage (Le Marrec, 1976; Vauchez and Buffalo, 1988). Migmatite in this outcrop lacks of mylonitic fabric, but shows open to tight F_2 folds (Fig. 24). The folds show subvertical axial planes oriented nearly N-S and sub-horizontal axes and are interpreted as developed during orogen-parallel transpression (Simonetti et al., 2020a). These structures are the outcrop-scale expression of upright large folds developed at the scale of the massif known as the Rouet antiform, the Reyran synform and the Cannes antiform (Crevola and Pupin, 1994; Demoux et al., 2008; Rolland et al., 2009; Corsini et al., 2010). In the Rouet antiform migmatitic gneiss displays a foliation trajectory with an irregular round shape and a stretching

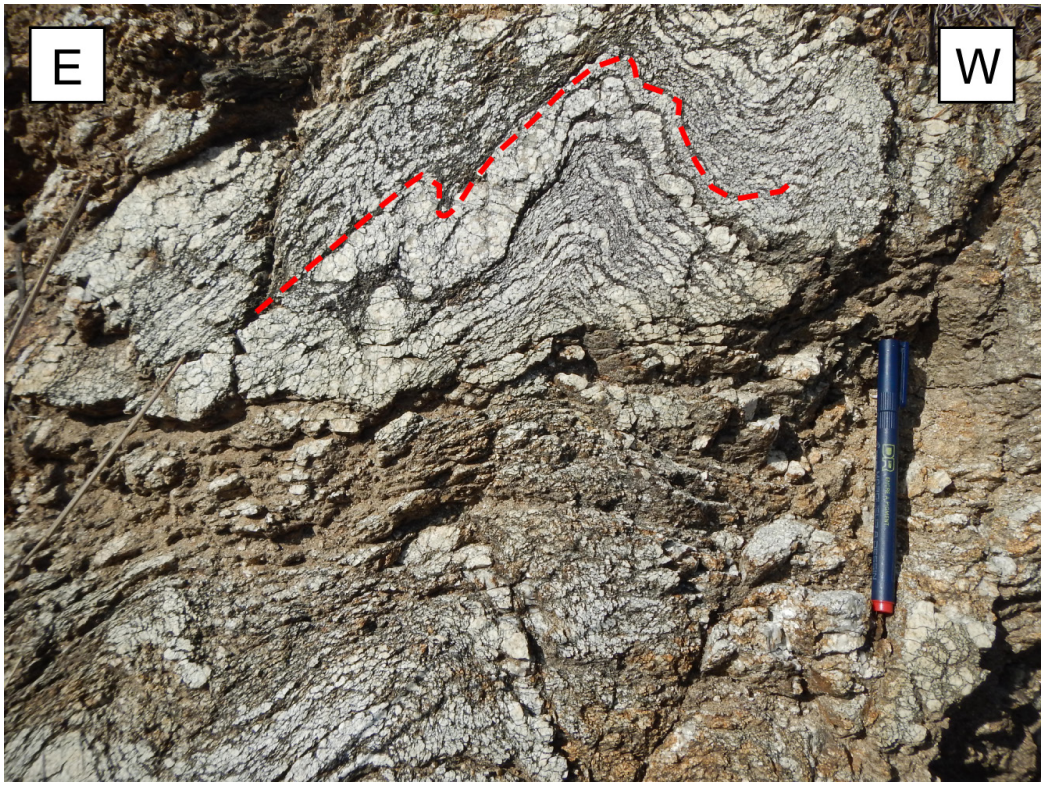

Fig. 24 - Migmatite of the Internal Zone belonging to the La Garde-Freinet unit exposed in stop 7 showing open to tight F_2 folds (red dashed line) with subvertical axial planes oriented nearly N-S and sub-horizontal axis.

https://doi.org/10.3301/GFT.2022.04

lineation trajectory with a radial pattern which was interpreted as a dome structure (Demoux et al., 2008; Rolland et al., 2009).

Stop 8 – Internal Zone, relations between the migmatite and the Plan-de-la-Tour granite
(coord. 43°18’ 01.6”N; 006°33’26.4”E)

From stop 7 we move northward following the D93 toward Saint Tropez and then following the D98A, the D559, the D224 roads and finally the D44 road, we reach the Plan-de-la-Tour locality. Stop 8 is located in an abandoned quarry on the left of the road (Fig. 5h). The car can be parked close to the outcrop.
Here the relationships between the migmatite and the Plan-de-la-Tour granite are visible. In particular, it is possible to observe leucocratic dikes related to the main intrusion crosscutting the foliation of the sourrounding rocks (Fig. 25).
Antiform structures in the Internal Zone are generally cored by late-orogenic granitoids structurally concordant with the surrounding migmatite (Rolland et al., 2009; Corsini et al., 2010; Schneider et al., 2014). The Plan-de-la-Tour granite is one of such intrusions. It derives from peraluminous magmas of crustal origin formed during the late Carboniferous orogenic-wide partial melting event. U-Th-Pb dating of monazite in the granite defined the crystallisation age of the grains during its emplacement, a process that started at 329 ± 3 My (Oliot et al., 2015) and that finished at the Carboniferous-Permian transition (Gerbault et al., 2018).

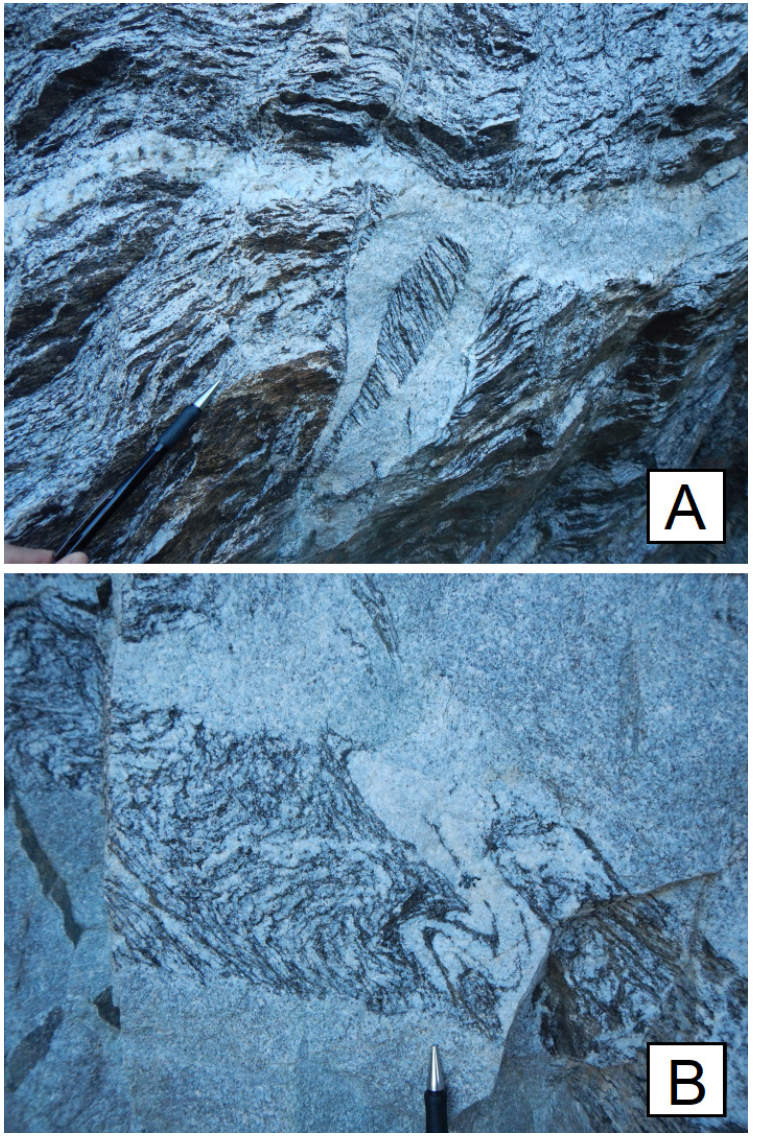

Fig. 25 - A) Cross-cutting relations between a leucocratic dike and migmatite of the Internal Zone; B) folded foliation in migmatitite crosscut by leucocratic dike; dikes and injections are related to the emplacement of the Plan-de-la-Tour granite.

https://doi.org/10.3301/GFT.2022.04

Acknowledgments

This field trip was prepared during the Phd of Matteo Simonetti and it was awarded of the "SGI best field trip 2021 award". Michel Corsini is greatly acknowledged for guiding me during the first phase of the field work and for the useful discussions. Rodolfo Carosi, Chiara Montomoli, Salvatore Iaccarino and Alessandro Petroccia are greatly thanked for their help, their support and for the useful discussion about the Maures Massif and the Variscan geology of the Mediterranean area. Eugenio Fazio and Salvatore Iaccarino are thanked for their revision that improved the quality of the paper. The manuscript also benefited from the constructive comments of Marco Scambelluri and Andrea Zanchi. This research was supported by funds from Torino University (Ricerca Locale 2017, 2018) and PRIN 2015 (resp. C. Montomoli).

https://doi.org/10.3301/GFT.2022.04

References

Advokaat E.L., van Hinsbergen D.J.J., Maffione M., Langereis C.G., Vissers R.L.M., Cherchi A., Schroeder R., Madani H., Columbu S. (2014) - Eocene rotation of Sardinia, and the paleogeography of the western Mediterranean region. Earth. Planet. Sc. Lett., 401, 183-195. https://doi.org/10.1016/j.epsl.2014.06.012

Arthaud F. and Matte P. (1977) - Late Paleozoic strikeslip faulting in southern Europe and northern Africa; result of a right-lateral shear zone between the Appalachians and the Urals. Geol. Soc. Am. Bull., 88, 1305-1320.

Ballèvre M., Bosse V., Ducassou C., Pitra P. (2009) - Palaeozoic history of the Armorican Massif: Models for the tectonic evolution of the suture zones. C. R. Geosci., 341, 174-201. https://doi.org/10.1016/j.crte.2008.11.009

Ballèvre M., Manzotti P., Dal Piaz G.V. (2018) - Pre-Alpine (Variscan) Inheritance: A Key for the Location of the Future Valaisan Basin (Western Alps). Tectonics, 37, 786-817. https://doi.org/10.1002/2017TC004633

Bellot J.-P. (2005) - The Palaeozoic evolution of the Maures massif (France) and its potential correlation with others areas of the Variscan belt: a review. J. Virtual Explor., 19. https://doi.org/10.3809/jvirtex.2005.00116

Bordet P. and Gueirard S. (1967) - Carte géologique de la France au 1/50,000 ième. Feuille de Saint-Tropez—Cap Lardier. BRGM eds

Briand B., Bouchardon J.-L., Capiez P., Piboule M. (2002) - Felsic (A-type)–basic (plume-induced) Early Palaeozoic bimodal magmatism in the Maures Massif (southeastern France). Geol. Mag., 139. https://doi.org/10.1017/S0016756802006477

Burg J.-P. and Matte P. (1978) A cross section through the French Massif Central and the scope of its Variscan Geodynamic Evolution. Zeitschrift Der Deutschen Geologischen Gesellschaft, 129, 429-460.

Buscail F. (2000) – Contributions à la compréhension du problème géologique et géodynamique des Maures: le métamorphisme régional modélisé dans le système KFMASH: analyse paragénétique, chémiographie, thermobarométrie, géochronologie Ar-Ar. PhD thesis, University of Montpellier II, France, 211 pp.

Carosi R., Montomoli C., Tiepolo M., Frassi C. (2012) - Geochronological constraints on post-collisional shear zones in the Variscides of Sardinia (Italy): Post-collisional shear zones in the Variscides of Sardinia. Terra Nova, 24, 42-51. https://doi.org/10.1111/j.1365-3121.2011.01035.x

Carosi R. and Palmeri R. (2002) Orogen-parallel tectonic transport in the Variscan belt of northeastern Sardinia (Italy): implications for the exhumation of medium-pressure metamorphic rocks. Geol. Mag., 139. https://doi.org/10.1017/S0016756802006763

Carosi R., Petroccia A., Iaccarino S., Simonetti M., Langone A., Montomoli C. (2020) - Kinematics and timing constraints in a transpressive tectonic regime: The example of the Posada-Asinara Shear Zone (NE Sardinia, Italy). Geosciences, 10, 288. https://doi.org/10.3390/geosciences10080288

Collombet M., Thomas J.C., Chauvin A., Tricart P., Bouillin J.P., Gratier J.P. (2002) - Counterclockwise rotation of the western Alps since the Oligocene: New insights from paleomagnetic data: tertiary rotation of the Western Alps. Tectonics, 21, 14-1-14-15. https://doi.org/10.1029/2001TC901016

Compagnoni R., Ferrando S., Lombardo B., Radulesco N., Rubatto D. (2010) - Paleo-European crust of the Italian Western Alps: Geological history of the Argentera Massif and comparison with Mont Blanc-Aiguilles Rouges and Maures-Tanneron Massifs. J. Virtual Explor., 36. https://doi.org/10.3809/jvirtex.2010.00228

Corsini M., Bosse V., Fe´raud G., Demoux A., Crevola G. (2010) - Exhumation processes during post-collisional stage in the Variscan belt revealed by detailed 40Ar/39Ar study (Tanneron massif, SE France). Int. J. Earth Sci. (Geol. Rundsch.), 96, 1-9.

Corsini M. and Rolland Y. (2009) - Late evolution of the southern European Variscan belt: Exhumation of the lower crust in a context of oblique convergence. C. R. Geosci., 341, 214-223. https://doi.org/10.1016/j.crte.2008.12.002

Crévola G. (1977) - Etude pétrographique et structurale de la partie orientale du massif du Tanneron (Provence cristalline). PhD thesis, University of Nice, France, 355 pp.

Crévola G. and Pupin J.-P. (1994) - Crystalline Provence: Structure and Variscan Evolution. In: Chantraine J., Rolet J., Santallier D.S., Piqué A., Keppie J.D. (Eds.), Pre-Mesozoic geology in France and related areas. Springer Berlin Heidelberg, Berlin, Heidelberg, 426-441

Demoux A., Scharer U., Corsini M. (2008) - Variscan evolution of the Tanneron massif, SE-France, examined through U–Pb monazite ages. J. Geol. Soc. London, 165, 467-478. https://doi.org/10.1144/0016-76492007-045

Di Vincenzo G., Carosi R., Palmeri R. (2004) - The Relationship between tectono-metamorphic evolution and Argon isotope records in white Mica: Constraints from in situ 40Ar-39Ar laser analysis of the Variscan Basement of Sardinia. J. Petrol., 45, 1013-1043. https://doi.org/10.1093/petrology/egh002

Dias R. and Ribeiro A. (1995) - The Ibero-Armorican Arc: A collision effect against an irregular continent? Tectonophysics, 246, 113-128. https://doi.org/10.1016/0040-1951(94)00253-6

Dias R., Ribeiro A., Romão J., Coke C., Moreira N. (2016) - A review of the arcuate structures in the Iberian Variscides; constraints and genetic models. Tectonophysics, 681, 170-194. https://doi.org/10.1016/j.tecto.2016.04.011

Faleiros F.M., Moraes R., Pavan M., Campanha G.A.C. (2016) - A new empirical calibration of the quartz c-axis fabric opening-angle deformation thermometer. Tectonophysics, 671, 173-182. https://doi.org/10.1016/j.tecto.2016.01.014

Faure M., Lardeaux J.-M., Ledru P. (2009) - A review of the pre-Permian geology of the Variscan French Massif Central. C. R. Geosci., 341, 202-213. https://doi.org/10.1016/j.crte.2008.12.001

Fernández-Lozano J., Pastor-Galán D., Gutiérrez-Alonso G., Franco P. (2016) - New kinematic constraints on the Cantabrian orocline: A paleomagnetic study from the Peñalba and Truchas synclines, NW Spain. Tectonophysics, 681, 195-208. https://doi.org/10.1016/j.tecto.2016.02.019

Fluck P., Piqué A., Schneider J.L., Whitechurch H. (1991) - Le socle vosgien. Sciences Géologiques 44, 207-235.

Gerbault M., Schneider J., Reverso-Peila A., Corsini M. (2018) - Crustal exhumation during ongoing compression in the Variscan Maures-Tanneron Massif, France-Geological and thermo-mechanical aspects. Tectonophysics, 746, 439-458. https://doi.org/10.1016/j.tecto.2016.12.019

Guillot S. and Ménot R.-P. (2009) - Paleozoic evolution of the External Crystalline Massifs of the Western Alps. C. R. Geosci., 341, 253-265. https://doi.org/10.1016/j.crte.2008.11.010

Innocent C., Michard A., Guerrot C., Hamelin B. (2003) - U-Pb zircon age of 548 Ma for the leptynites (high-grade felsic rocks) of the central part of the Maures Massif. Geodynamic significance of the so-called leptyno-amphibolitic complexes of the Variscan belt of western Europe. Bull. Soc. Géol. Fr., 174, 585-594.

Lancelot J., Moussavou M., Delor C. (1998) - Geochronologie U/Pb des temoins de l'evolution ante-varisque du massif des Maures. BRGM-SGF special meeting: Géologie du massif des Maures, Le Plan-de-la Tour, France, p. 22.

Law R.D. (2010) - Moine Thrust zone mylonites at the Stack of Glencoul: II—results of vorticity analyses and their tectonic significance. Geol. Soc. Lond. Spec. Publ., 335, 579-602. https://doi.org/10.1144/SP335.24

Law R.D. (2014) - Deformation thermometry based on quartz c-axis fabrics and recrystallization microstructures: a review. J. Struct. Geol., 66, 129-161. https://doi.org/10.1016/j.jsg.2014.05.023

Law R.D., Searle M.P., Simpson R.L. (2004) - Strain, deformation temperatures and vorticity of flow at the top of the greater Himalayan Slab, Everest Massif, Tibet. J. Geol. Soc. Lond., 161, 305-320. https://doi.org/10.1144/0016-764903-047

Le Marrec A. (1976) - Reconnaissance pétrographique et structurale des formations cristallophylliennes catazonales du massif de Sainte-Maxime (quart NE du massif varisque des Maures, Var, France). MsC Thesis, University of Aix-Marseille 3, France, 126 pp.

Maquil R. (1976) - Contribution à l'étude pétrographique et structurale de la région SE du massif des Maures (Var, France). Annale de la Société Géologique de Belgique, 99, 601-613.

Matte P. (1986) - La Chaîne varisque parmi les chaînes paléozoïques péri-atlantiques, modèle d'évolution et position des grands blocs continentaux au Permo-Carbonifère. Bull. Soc. Géol. Fr., 8, 4-24.

Matte P. (2001) - The Variscan collage and orogeny (480–290 Ma) and the tectonic definition of the Armorica microplate: a review. Terra Nova, 13, 122-128. https://doi.org/10.1046/j.1365-3121.2001.00327.x

Moussavou M. (1998) - Contribution à l'histoire thermo-tectonique varisque du massif des Maures par la typologie du zircon et la géochronologie U/Pb sur minéraux accessoires. Doctorate thesis, pp 187. University of Montpellier 2.

Oliot E., Melleton J., Schneider J., Corsini M., Gardien V., Rolland Y. (2015) - Variscan crustal thickening in the Maures-Tanneron massif (South Variscan belt, France): new in situ monazite U-Th-Pb chemical dating of high-grade rocks. Bull. Soc. Géol. Fr., 186, 145-169. https://doi.org/10.2113/gssgfbull.186.2-3.145

Padovano M., Dörr W., Elter F.M., Gerdes A. (2014) - The East Variscan Shear Zone: Geochronological constraints from the Capo Ferro area (NE Sardinia, Italy). Lithos, 196-197, 27-41. https://doi.org/10.1016/j.lithos.2014.01.015

Padovano M., Elter F.M., Pandeli E., Franceschelli M. (2012) - The East Variscan Shear Zone: new insights into its role in the Late Carboniferous collision in southern Europe. Int. Geol. Rev., 54, 957-970. https://doi.org/10.1080/00206814.2011.626120

Ramsay J.G. and Huber M.I. (1987) - The Techniques of Modern Structural Geology, Vol. 2: Folds and Fractures. Academic Press, London.

Rolland Y., Corsini M., Demoux A. (2009) - Metamorphic and structural evolution of the Maures-Tanneron massif (SE Variscan chain): evidence of doming along a transpressional margin. Bull. Soc. Géol. Fr., 180, 217-230. https://doi.org/10.2113/gssgfbull.180.3.217

https://doi.org/10.3301/GFT.2022.04

Rosenbaum G., Lister G.S., Duboz C. (2002) - Reconstruction of the tectonic evolution of the western Mediterranean since the Oligocene. J. Virtual Explor., 08. https://doi.org/10.3809/jvirtex.2002.00053

Schmid S.M. and Casey M. (1986) - Complete fabric analysis of some commonly observed quartz C-axis patterns. In: Hobbs B.E., Heard H.C. (Eds.), Geophysical Monograph Series, vol. 36. American Geophysical Union, Washington D.C, pp. 263-286.

Schneider J., Corsini M., Reverso-Peila A., Lardeaux J.-M. (2014) - Thermal and mechanical evolution of an orogenic wedge during Variscan collision: an example in the Maures–Tanneron Massif (SE France). Geol. Soc. Spec. Publ., 405, 313-331. https://doi.org/10.1144/SP405.4

Schulmann K., Konopásek J., Janoušek V., Lexa O., Lardeaux J.-M., Edel J.-B., Štípská P., Ulrich S. (2009) - An Andean type Palaeozoic convergence in the Bohemian Massif. C. R. Geosci., 341, 266-286. https://doi.org/10.1016/j.crte.2008.12.006

Simonetti M., Carosi R., Montomoli C., Langone A., D'Addario E., Mammoliti E. (2018) - Kinematic and geochronological constraints on shear deformation in the Ferriere-Mollières shear zone (Argentera-Mercantour Massif, Western Alps): implications for the evolution of the Southern European Variscan Belt. Int. J. Earth Sci., 107, 2163-2189. https://doi.org/10.1007/s00531-018-1593-y

Simonetti M., Carosi R., Montomoli C., Corsini M., Petroccia A., Cottle J.M., Iaccarino S. (2020a) - Timing and kinematics of flow in a transpressive dextral shear zone, Maures Massif (Southern France). Int. J. Earth Sci., 109, 2261-2285. https://doi.org/10.1007/s00531-020-01898-6

Simonetti M., Carosi R., Montomoli C., Cottle J.M., Law R.D. (2020b) - Transpressive deformation in the Southern European Variscan Belt: new insights From the Aiguilles Rouges Massif (Western Alps). Tectonics, 39. https://doi.org/10.1029/2020TC006153

Simonetti M., Carosi R., Montomoli C., Iaccarino S. (2021a) - The role of regional-scale shear zones in paleogeographic reconstructions: the case study of the Variscan belt in the Mediterranean area, EGU General Assembly 2021, online, 19-30 Apr 2021, EGU21-8673. https://doi.org/10.5194/egusphere-egu21-8673

Simonetti M., Carosi R., Montomoli C., Law R.D., Cottle J.M. (2021b) Unravelling the development of regional-scale shear zones by a multidisciplinary approach: The case study of the Ferriere-Mollières Shear Zone (Argentera Massif, Western Alps). J. Struct. Geol., 149, 104399. https://doi.org/10.1016/j.jsg.2021.104399

Skrzypek E., Štípská P., Cocherie A. (2012) - The origin of zircon and the significance of U–Pb ages in high-grade metamorphic rocks: a case study from the Variscan orogenic root (Vosges Mountains, NE France). Contrib. to Mineral. Petrol., 164, 935-957. https://doi.org/10.1007/s00410-012-0781-1

Stampfli G.M., Borel G.D., Marchant R., Mosar J. (2002) - Western Alps geological constraints on western Tethyan reconstructions. J. Virtual. Explor. 8, 77.

Stampfli G.M. and Kozur H.W. (2006) - Europe from the Variscan to the Alpine cycles. Geol. Soc. Lond. Mem., 32, 57-82. https://doi.org/10.1144/GSL.MEM.2006.032.01.04

Tollmann A. (1982) - Großraumiger variszischer Deckenbau im Moldanubikum und neue Gedanken zum Variszikum Europas. Geotektonische Forschungen 64, 1-91.

https://doi.org/10.3301/GFT.2022.04

Turco E., Macchiavelli C., Mazzoli S., Schettino A., Pierantoni P.P. (2012) - Kinematic evolution of Alpine Corsica in the framework of Mediterranean mountain belts. Tectonophysics, 579, 193-206. https://doi.org/10.1016/j.tecto.2012.05.010

Vauchez A. (1987) - Mécanismes de déformation et cinématique des zones de mouvements ductiles. PhD thesis, University of Aix-Marseille 3, France, 313 pp.

Vauchez A. and Bufalo M. (1988) - Charriage crustal, anatexie et décrochements ductiles dans les Maures orientales (Var, France) au cours de l'orogenèse varisque. Geol. Rundsch., 77, 45-62.

Wallis S.R., Platt J.P, Knott S.D. (1993) - Recognition of synconvergence extension in accretionary wedges with examples from the Caiabrian Arc and the Eastern Alps. Am. J. Sci., 293, 463-495.

Manuscript received 11 November 2021; accepted 21 March 2022; published online 1 July 2022;
editorial responsibility and handling by M. Scambelluri.

https://doi.org/10.3301/GFT.2022.04